Coordination Complexes of Transition Metals (M = Mo, Fe, Rh, and Ru) with Tin(II) Phthalocyanine in Neutral, Monoanionic, and Dianionic States

AUTHOR(S):

Konarev, Dmitri V.; Kuzmin, Alexey V.; Nakano, Yoshiaki; Faraonov, Maxim A.; Khasanov, Salavat S.; Otsuka, Akihiro; Yamochi, Hideki; Saito, Gunzi; Lyubovskaya, Rimma N.

CITATION:

Konarev, Dmitri V. ...[et al]. Coordination Complexes of Transition Metals (M = Mo, Fe, Rh, and Ru) with Tin(II) Phthalocyanine in Neutral, Monoanionic, and Dianionic States. Inorganic Chemistry 2016, 55(4): 1390-1402

ISSUE DATE:

2016-02-02

URL:

http://hdl.handle.net/2433/219606

Coordination complexes of transition metals (M = Mo, Fe, Rh, and Ru) with tin(II) phthalocyanine in neutral, monoanionic, and dianionic states

Dmitri V. Konarev,*† Alexey V. Kuzmin,‡ Yoshiaki Nakano,§ Maxim A. Faraonov,† Salavat S. Khasanov,‡ Akihiro Otsuka,§ Hideki Yamochi,§ Gunzi Saito,||, ¶ and Rimma N. Lyubovskaya†

†Institute of Problems of Chemical Physics RAS, Chernogolovka, Moscow region, 142432 Russia;

‡Institute of Solid State Physics RAS, Chernogolovka, Moscow region, 142432 Russia;

§Research Center for Low Temperature and Materials Sciences, Kyoto University, Sakyo-ku, Kyoto 606-8501, Japan;

||Faculty of Agriculture, Meijo University, 1-501 Shiogamaguchi, Tempaku-ku, Nagoya 468-8502, Japan.

¶Toyota Physical and Chemical Research Institute, 41-1, Yokomichi, Nagakute, Aichi 480-1192, Japan

Abstract–The ability of tin atoms to form stable Sn−M bonds with transition metals was used to prepare transition metal complexes with tin(II) phthalocyanine in neutral, monoanionic, and dianionic states. These complexes were obtained via the interactions of $[Sn^{IV}Cl_2Pc(3-)]^{\bullet-}$ or $[Sn^{II}Pc(3-)]^{\bullet-}$ radical anions with $\{Cp^*Mo(CO)_2\}_2$, $\{CpFe(CO)_2\}_2$, $\{CpMo(CO)_3\}_2$, $Fe_3(CO)_{12}$, $\{Cp^*RhCl_2\}_2$, or $Ph_5CpRu(CO)_2Cl$. The neutral coordination complexes of $Cp^*MoBr(CO)_2[Sn^{II}Pc(2-)]\cdot 0.5C_6H_4Cl_2$ (**1**) and $CpFe(CO)_2[Sn^{II}Pc(2-)]\cdot 2C_6H_4Cl_2$ (**2**) were obtained from $[Sn^{IV}Cl_2Pc(3-)]^{\bullet-}$. On the other hand, the coordination of transition metals to $[Sn^{II}Pc(3-)]^{\bullet-}$ yielded anionic coordination complexes and preserving the spin on $[Sn^{II}Pc(3-)]^{\bullet-}$. However, in the case of $\{cryptand[2,2,2](Na^+)\}\{CpFe^{II}(CO)_2[Sn^{II}Pc(4-)]\}^-\cdot C_6H_4Cl_2$ (**4**), charge transfer from $CpFe^{I}(CO)_2$ to $[Sn^{II}Pc(3-)]^{\bullet-}$ took place to form the diamagnetic $[Sn^{II}Pc(4-)]^{2-}$ dianion and $\{CpFe^{II}(CO)_2\}^+$. The complexes $\{cryptand[2,2,2](Na^+)\}\{Fe(CO)_4[Sn^{II}Pc(3-)]^{\bullet-}\}$ (**5**),

{cryptand[2,2,2](Na$^+$)} {CpMo(CO)$_2$[Sn^{II}Pc(2-)Sn^{II}Pc(3-)$^{\bullet-}$]} (**6**), and {cryptand[2,2,2](Na$^+$)} {Cp*RhCl$_2$[Sn^{II}Pc(3-)]$^{\bullet-}$} (**7**) have the magnetic moments of 1.75 μ_B, 2.41 μ_B, and 1.75 μ_B, respectively, owing to the presence of S = 1/2 spins on [Sn^{II}Pc(3-)]$^{\bullet-}$ and CpMo^{I}(CO)$_2$ (for **6**). In addition, the strong antiferromagnetic coupling of spins with Weiss temperatures of −27.6 K and −28.6 K was realized between the CpMo^{I}(CO)$_2$ and [Sn^{II}Pc(3-)]$^{\bullet-}$ units in **6** and the π-stacking {Fe(CO)$_4$[Sn^{II}Pc(3-)]$^{\bullet-}$}$_2$ dimers of **5**, respectively. The [Sn^{II}Pc(3-)]$^{\bullet-}$ radical anions substituted the chloride anions in Ph$_5$CpRu(CO)$_2$Cl to form the formally neutral compound {Ph$_5$CpRu^{II}(CO)$_2$[Sn^{II}Pc(3-)]} (**8**) in which the negative charge and spin are preserved on [Sn^{II}Pc(3-)]$^{\bullet-}$. The strong antiferromagnetic coupling of spins with a magnetic exchange interaction J/k_B = −183 K in **8** is explained by the close packing of [Sn^{II}Pc(3-)]$^{\bullet-}$ in the π-stacked {Ph$_5$CpRu^{II}(CO)$_2$[Sn^{II}Pc(3-)]$^{\bullet-}$}$_2$ dimers.

*Correspondence to: Dmitri V. Konarev, e-mail: konarev@icp.ac.ru, fax: +7 49652-21852.

Introduction

Metal phthalocyanines (Pcs) and porphyrins are used for the preparation of photoactive, magnetic, and conducting compounds.[1] The coordination of transition metals to metal macroheterocycles can affect their electronic structures and properties, and these complexes are thus of special interest.[2-5] Transition metals coordinate via η^6-type bonding to the isoindole subunits of the Pc ligands as in {Cp*Ru[η^6-Ni(PcOEt)]}PF$_6$, which was obtained via the interaction of metal octa(ethoxy)phthalocyanine M(PcOEt) (M = H$_2$, Ni, Cu, VO) with [Cp*Ru(MeCN)$_3$]PF$_6$ (Cp* = 1,2,3,4,5-pentamethylcyclopentadienyl).[2] In addition, the η^5-type complexes of zinc and nickel octaethylporphyrin with (cymene)Ru^{2+} and Cp*Ir^{2+} have been obtained and structurally characterized.[3] The transition metal complexes of metal macroheterocycles can also be prepared

with metal–metal bonds, such as those observed in phthalocyanine and porphyrin dimers.[6] Manganese, cobalt, molybdenum, and osmium in the form of carbonyl (CO) and cyclopentadienyl (Cp) complexes have been shown to coordinate to the central metal atoms of indium, thallium, and tin tetraphenylporphyrins.[4] Two coordination compounds were obtained as powders following the reaction of tin phthalocyanine: $Fe(CO)_4(SnPc)$ and $[Re(CO)_3]_2(SnPc)$.[5] Recently, we prepared $(Cp^*Ir^{III}I_2)[Sn^{II}Pc(2-)]\cdot 2C_6H_4Cl_2$, the first crystalline neutral coordination complex in which two metal-containing fragments are bound via an Sn–Ir bond with a length of 2.58 Å.[7] Thus, transition metal complexes are obtained from neutral metal porphyrins and phthalocyanines.[5-7] However, such complexes with radical anions of metal phthalocyanine remain unknown, and synthetic routes for their preparation have not yet been developed.

Insoluble-unsubstituted metal phthalocyanines become soluble in organic solvents under reducing conditions,[8] allowing the reaction investigations of metal phthalocyanine radical anions with transition metals. The interactions of $(cation^+)[Sn^{IV}Cl_2Pc(3-)]^{\bullet-}$ (cation = Bu_4N^+ or cryptand[2,2,2](Na^+)) and $\{cryptand[2,2,2](Na^+)\}[Sn^{II}Pc(3-)]^{\bullet-}$ (henceforth, cryptand[2,2,2] is abbreviated to cryptand) with transition metal compounds result in the direct coordination of these complexes to tin(II) phthalocyanine to form neutral (**1**, **2**), monoanionic (**5**–**8**), and even dianionic (**4**) coordination complexes, in some of which the spin on $[Sn^{II}Pc(3-)]^{\bullet-}$ is preserved (**5**–**8**, Table 1). Thus, $[Sn^{II}Pc(3-)]^{\bullet-}$ radical anions are new paramagnetic anionic ligands for transition metals. Herein, we describe the synthesis, molecular structures, and optical and magnetic properties of these complexes. The optical and magnetic properties of the salt $\{cryptand(Na^+)\}[Sn^{II}Pc(3-)]^{\bullet-}\cdot C_6H_4Cl_2$ (**3**) were also studied and compared with those of the transition metal complexes. The developed approach offers new possibilities for the design of magnetic and conducting assemblies based on metal phthalocyanines and transition metals.

Table 1. Starting compounds for the syntheses of **1**–**8** and compositions of obtained compounds.

№	Starting compounds Phthalocyanine*	Transition metal complex	Composition of the obtained complexes
1	$[Sn^{IV}Cl_2Pc(3-)]^{\bullet-}$	$\{Cp^*Mo(CO)_2\}_2$	$Cp^*Mo^{II}Br(CO)_2[Sn^{II}Pc(2-)]\cdot 0.5C_6H_4Cl_2$
2	$[Sn^{IV}Cl_2Pc(3-)]^{\bullet-}$	$\{CpFe(CO)_2\}_2$	$CpFe^{I}(CO)_2[Sn^{II}Pc(2-)]\cdot 2C_6H_4Cl_2$
3	$[Sn^{II}Pc(3-)]^{\bullet-}$		$\{cryptand(Na^+)\}[Sn^{II}Pc(3-)]^{\bullet-}\cdot C_6H_4Cl_2$
4	$[Sn^{II}Pc(3-)]^{\bullet-}$	$\{CpFe(CO)_2\}_2$	$\{cryptand(Na^+)\}\{CpFe^{II}(CO)_2[Sn^{II}Pc(4-)]\}^{-}\cdot 1.5C_6H_4Cl_2$
5	$[Sn^{II}Pc(3-)]^{\bullet-}$	$Fe_3(CO)_{12}$	$\{cryptand(Na^+)\}\{Fe^0(CO)_4[Sn^{II}Pc(3-)]^{\bullet-}\}\cdot 1/3C_6H_4Cl_2$
6	$[Sn^{II}Pc(3-)]^{\bullet-}$	$\{CpMo(CO)_3\}_2$	$\{cryptand(Na^+)\}\{CpMo^{I}(CO)_2[(Sn^{II}Pc(2-)(Sn^{II}Pc(3-)^{\bullet-}]\}\cdot 3.5C_6H_4Cl_2$
7	$[Sn^{II}Pc(3-)]^{\bullet-}$	$(Cp^*RhCl_2)_2$	$\{cryptand(Na^+)\}\{Cp^*Rh^{III}Cl_2[Sn^{II}Pc(3-)]^{\bullet-}\}\cdot C_6H_4Cl_2$
8	$[Sn^{II}Pc(3-)]^{\bullet-}$	$Ph_5CpRu(CO)_2Cl$	$Ph_5CpRu^{II}(CO)_2[Sn^{II}Pc(3-)]$

Formal oxidation state of metals is shown.
*Salts with cryptand(Na^+) counter cations were used for all of the syntheses, except for complex **1**, which was prepared using $(Bu_4N^+)[Sn^{IV}Cl_2Pc(3-)]^{\bullet-}$.

RESULTS AND DISCUSSION

Synthesis

$[Sn^{IV}Cl_2Pc(2-)]^0$ and $[M^{II}Pc(2-)]^0$ can be reduced at reasonable redox potentials (approximately −0.52 and −0.4– −0.8 V *vs.* SCE, respectively).[9] The reduction of $[Sn^{IV}Cl_2Pc(2-)]^0$ and $[Sn^{II}Pc(2-)]^0$ with sodium fluorenone ketyl in the presence of an excess of $(Bu_4N^+)(Br^-)$ or one equivalent of cryptand yielded the soluble, deep-blue salts $(cation^+)[Sn^{IV}Cl_2Pc(3-)]^{\bullet-}$ (cation = Bu_4N^+ or cryptand(Na^+)) and $\{cryptand(Na^+)\}[Sn^{II}Pc(3-)]^{\bullet-}$. The salts with cryptand(Na^+) counter cations were crystallized as $\{cryptand(Na^+)\}[Sn^{II}Pc(3-)]^{\bullet-}\cdot C_6H_4Cl_2$ (**3**) and $\{cryptand(Na^+)\}[Sn^{IV}Cl_2Pc(3-)]^{\bullet-}\cdot C_6H_4Cl_2$, and here, we present the crystal structure and properties of **3**. When the $[Sn^{IV}Cl_2Pc(3-)]^{\bullet-}$ and $[Sn^{II}Pc(3-)]^{\bullet-}$ radical anions were allowed to interact with $\{Cp^*Mo(CO)_2\}_2$, $\{CpFe(CO)_2\}_2$, $\{CpMo(CO)_3\}_2$, $Fe_3(CO)_{12}$, $\{Cp^*RhCl_2\}_2$, or $Ph_5CpRu(CO)_2Cl$, the crystals of the corresponding transition metal complexes of neutral and anionic tin(II) phthalocyanine were obtained (see Table 1 for the compositions of the complexes).

When the (cation^{+})[$Sn^{IV}Cl_2Pc(3-)]^{\bullet-}$ salts (cation = Bu_4N^{+} or cryptand(Na^{+})) were reacted with $\{Cp^*Mo(CO)_2\}_2$ and $\{CpFe(CO)_2\}_2$, an immediate color change from deep blue to green or greenish-blue, respectively, was observed, which is the characteristic of neutral coordination complexes of tin(II) phthalocyanine, such as $Cp^*Ir^{III}I_2[Sn^{II}Pc(2-)]\cdot 2C_6H_4Cl_2$.[7] The color changes indicated that the coordination of the transition metal was accompanied by the oxidation of the $[Sn^{IV}Cl_2Pc(3-)]^{\bullet-}$ radical anions. This oxidation most likely occurs via the transition of Sn^{IV} to Sn^{II} with the elimination of the chloride anions, followed by the coordination of the transition metal to the tin(II) atom of $Sn^{II}Pc(2-)$. Therefore, this synthetic route through $[Sn^{IV}Cl_2Pc(3-)]^{\bullet-}$ is useful for the preparation of neutral coordination complexes of tin(II) phthalocyanine. Because the excesses of the transition metal compounds $\{Cp^*Mo(CO)_2\}_2$ and $\{CpFe(CO)_2\}_2$ are used in the syntheses, these complexes can also participate in redox reactions, specifically the oxidation of Sn^{IV} to Sn^{II} with the acceptance of a halide anion to form, for example, $Cp^*Mo^{II}Br(CO)_2$ and $CpFe^{II}Cl(CO)_2$. In the case of **1**, $Cp^*Mo^{II}Br(CO)_2$ is coordinated to $Sn^{II}Pc(2-)$ (the length of the Mo–Br bond in **1** is the characteristic of Mo–Br bonds in other Cp(*)Mo compounds).[11,12] The excess of (Bu_4N^{+})(Br^{-}) in the reaction solutions leads to the substitution of Cl^{-} by Br^{-} to form $[Sn^{IV}Br_2Pc(3-)]^{\bullet-}$ and explains the presence of Br^{-} rather than Cl^{-} in **1**. A similar substitution was observed during the formation of salts with indium(III) bromide phthalocyanine radical anions ($[In^{III}BrPc(3-)]^{\bullet-}$).[8d]

The reaction of {cryptand(Na^{+})}$[Sn^{II}Pc(3-)]^{\bullet-}$ with $\{CpFe(CO)_2\}_2$ to form **4** was accompanied by a slow color change (over several hours) from deep blue to violet, indicating that the $[Sn^{II}Pc(3-)]^{\bullet-}$ radical anions disappeared following the coordination of $CpFe(CO)_2$, most likely owing to charge transfer between them (see below).

Following the addition of $Fe_3(CO)_{12}$, $\{CpMo(CO)_3\}_2$, $(Cp^*RhCl_2)_2$, or $Ph_5CpRu(CO)_2Cl$, the solutions of {cryptand(Na^{+})}$[Sn^{II}Pc(3-)]^{\bullet-}$ remained blue, indicating that the $[Sn^{II}Pc(3-)]^{\bullet-}$ radical

anions were preserved in **5**–**8**, even after the coordination of these transition metals to $[Sn^{II}Pc(3-)]^{\bullet-}$.

In the case of compound **8**, the $[Sn^{II}Pc(3-)]^{\bullet-}$ radical anion substituted the halogen at the metal center of $Ph_5CpRu(CO)_2Cl$ to form the formally neutral compound $Ph_5CpRu(CO)_2[Sn^{II}Pc(3-)]$, which, however, still contained $[Sn^{II}Pc(3-)]^{\bullet-}$ as a ligand.

Spectroscopic properties

The charged state of a $Sn^{II}Pc$ complex can be estimated by anazlyzing its ultraviolet (UV)–visible–near-infrared (NIR) spectrum, because the formation of $[Sn^{II}Pc(3-)]^{\bullet-}$ is accompanied by noticeable changes in the optical properties of tin(II) phthalocyanine. The spectrum of the starting $[Sn^{II}Pc(2-)]^0$ unit shows absorption bands at 342 (Soret band), 558, 729, and 852 nm (Q-bands), and no absorption bands are observed in the NIR range above 900 nm (Fig. 1). The spectrum of $[Sn^{II}Pc(2-)]^0$ in the solution shows an essentially narrower Soret and Q-bands centered at 302, 359 nm and 616, 682 nm, respectively.[10] The formation of $Sn^{II}Pc(3-)^{\bullet-}$ in previously studied $(Bu_4N^+)_2[Sn^{II}Pc(3-)]^{\bullet-}(Br^-)\cdot 0.5C_6H_4Cl_2\cdot 0.5C_6H_{14}$ and $(Et_4N^+)[Sn^{II}Pc(3-)]^{\bullet-}\cdot 1.5C_6H_4Cl_2$[8e] and newly obtained **3** is

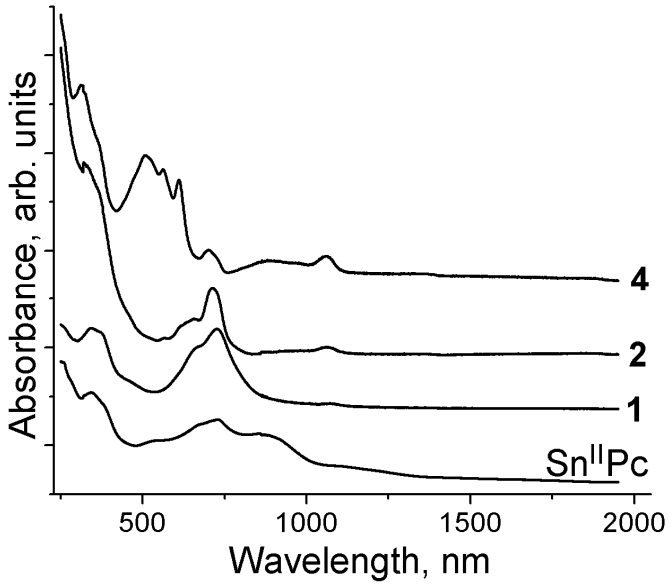

Figure 1. Spectra of $[Sn^{II}Pc(2-)]^0$, neutral complexes **1** and **2** (c), and anionic complex **4** containing $[Sn^{II}Pc(4-)]^{2-}$ dianion, obtained using KBr pellets prepared under anaerobic conditions.

Table 2. Data for the UV–visible–NIR spectra of $Sn^{II}Pc(2-)$, salt **3**, and their neutral and anionic coordination complexes with transition metals (Figs. 1 and 2) obtained using KBr pellets.

Compound	Position of phthalocyanine absorption bands, nm		
	Soret band	Q-band	Bands attributed to the radical anion
$Sn^{II}Pc(2-)$	342	558, 668, 726 (max), 852	-
$Sn^{II}Pc(2-)$ in ethanol[10]	302, 359	616, 682	-
1	340	665, 726 (max)	-
2	321	649, 714 (max)	- 1062 (weak)
3	337	560, 649 (max)	890 (weak), 1032
4	315	508 (max), 560, 610, 704	900 (weak), 1063 (weak)
5	334	613 (max), 722	863, 1050
6	340	660, 714 (max)	904 (weak), 1042
7	338	638,726 (max)	854 (weak), 1038
8	343	618, 730 (max)	893 (weak), 1063

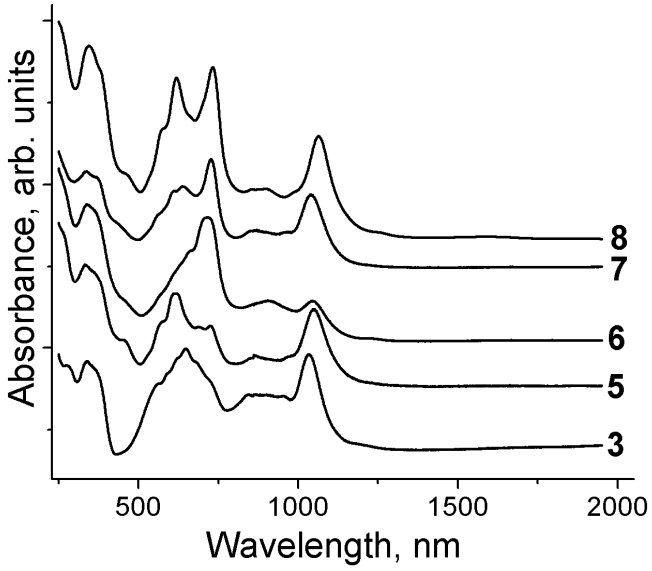

Figure 2. UV–visible–NIR spectra of salt **3** and coordination complexes **5**, **6**, **7**, and **8** containing $[Sn^{II}Pc(3-)]^{\bullet-}$ radical anion, obtained using KBr pellets prepared under anaerobic conditions.

accompanied by the appearance of new intense bands in the NIR region at 1032–1041 nm, along with weaker absorption bands at 840–890 nm (Fig. 2). The appearance of these bands unambiguously indicates the formation of $[Sn^{II}Pc(3-)]^{\bullet-}$.

The spectra of **1** and **2** are shown in Fig. 1. It can be seen in the figures that absorption bands in the NIR region are very weak or absent from these spectra, indicating the existence of the neutral state $[Sn^{II}Pc(2-)]^{0}$ in these complexes. The shapes and positions of the Q-bands in the spectra of **1** and **2** (Table 1, Fig. 1) are also very close to those in the spectrum of $(Cp^{*}Ir^{III}I_2)[Sn^{II}Pc(2-)]\cdot 2C_6H_4Cl_2$, which contains neutral $[Sn^{II}Pc(2-)]^{0}$.[7]

Complex **4**, which contains a negatively charged $\{CpFe(CO)_2[Sn^{II}Pc]\}^{-}$ anion, yielded an unusual spectrum, with rather weak absorption bands at 900 and 1063 nm (Fig. 1), indicating the absence of the $[Sn^{II}Pc(3-)]^{\bullet-}$ radical anion. The violet color of **4** in the solid state also supports this assumption, because all of the salts with $[Sn^{II}Pc(3-)]^{\bullet-}$ ligands are deep blue in color.[8e] Most likely, the charge transfer between the initial $[Sn^{II}Pc(3-)]^{\bullet-}$ and $CpFe^{I}(CO)_2$ reagents occurred in **4** to form either (A) neutral $[Sn^{II}Pc(2-)]^{0}$ and $\{CpFe^{0}(CO)_2\}^{-}$ anions or (B) $[Sn^{II}Pc(4-)]^{2-}$ dianions and $\{CpFe^{II}(CO)_2\}^{+}$ cations. In both cases, $\{CpFe(CO)_2[Sn^{II}Pc]\}^{-}$ anions result. Charge transfer is accompanied by large blue shifts of the Q-bands of phthalocyanine to 508 nm (max), 560 nm, and 610 nm, whereas the intensity of the band at 704 nm decreases (Fig. 1). The Soret band is also blue-shifted in the spectrum of **4** from 342 nm to 315 nm. These results suggest that pathway (B) occurred, because the positions of the absorption bands for $Sn^{II}Pc$ in the spectrum of **4** are not coincident with those characteristic of the neutral $[Sn^{II}Pc(2-)]^{0}$ ligands in the spectra of **1** and **2**. Previously, we found that the formation of negatively charged metal phthalocyanines is accompanied by the noticeable blue shifts of the Soret and Q-bands.[8e] Blue shifts are also observed for the $[Sn^{II}Pc(4-)]^{2-}$ dianions.

The spectra of **5**–**7** presented in Fig. 2 show intense bands in the NIR region with maxima at 1038–1048 nm and weaker bands at 854–908 nm, indicating the presence of $[Sn^{II}Pc(3-)]^{\bullet-}$. The

intensities of these NIR bands in the spectra of **5** and **7** are comparable to those of the Q-bands in the spectrum of **3** (Fig. 2), while the band at 1048 nm in the spectrum of **6** is almost two times less intense than those of the Q-bands (Fig. 2). These results can be explained by the presence of two $Sn^{II}Pc$ units per one cryptand(Na^+) cation in **6**; only one of two $Sn^{II}Pc$ units has a charge of −1 (the other is neutral), and thus, the charge disproportionation is observed, or −1 charge, is delocalized over two $Sn^{II}Pc$ moieties. The spectrum of **6** in the visible–NIR and IR regions is more consistent with the charge disproportionation.

In the spectrum of the neutral coordination complex **8**, an intense NIR band at 1063 nm and a weaker band at 893 nm were observed, indicating the retention of $[Sn^{II}Pc(3-)]^{\bullet-}$ after its coordination with $Ph_5CpRu(CO)_2$.

The formation of the $[Sn^{II}Pc(3-)]^{\bullet-}$ salts was also accompanied by the blue shifts of the Q- and Soret bands compared with the locations of these peaks in the spectrum of neutral $[Sn^{II}Pc(2-)]^0$.[8e] However, no such effect was observed for the coordination complexes with $[Sn^{II}Pc(3-)]^{\bullet-}$. All of the spectra of these complexes exhibited two Q-bands with maxima at 617–658 nm and 714–736 nm. Only in the spectrum of **6** band at 617–658 nm is weak (Fig. 2). In addition, no measurable differences in the positions of the Soret bands (315–340 nm and 332–343 nm) were detected in the

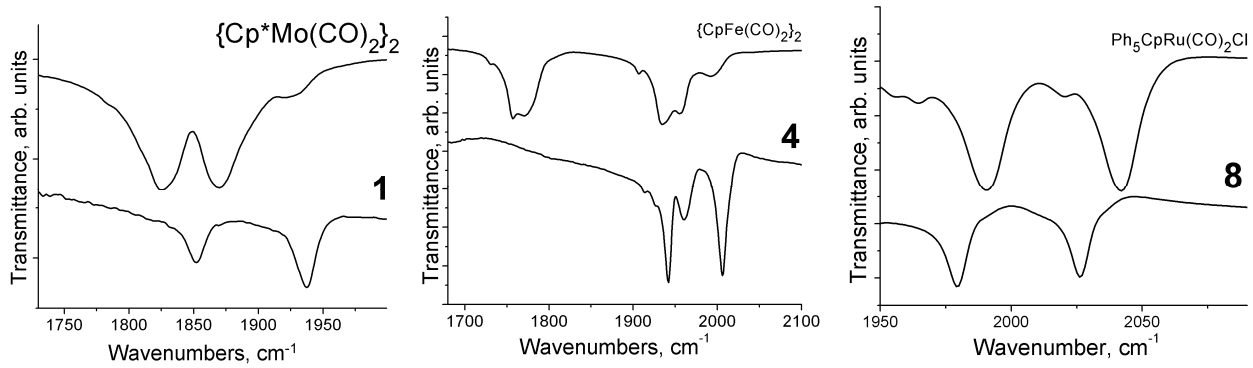

Figure 3. IR spectra of starting compounds and complexes **1**, **4**, and **8** in the range of the CO stretching vibrations.

spectra of the coordination complexes with $[Sn^{II}Pc(2-)]^0$ and $[Sn^{II}Pc(3-)]^{\bullet-}$.

The key bands in the IR spectra of the starting compounds, salt **3**, and coordination complexes **1**, **2**, and **4**–**8** are listed in Tables S1–S3 and presented in Figs. S1–S8. Most of the transition metal complexes used in the present study contained carbonyl ligands. The positions of the CO stretching modes in the IR spectra of metal carbonyls are very sensitive to the charged states of the metal centers, with shifts to lower or higher frequencies upon reduction or oxidation, respectively. Indeed, the CO stretching modes for the $\{Cp^*Mo(CO)_2\}_2$ dimers at 1825 and 1870 cm^{-1} are shifted to 1852 and 1937 cm^{-1}, respectively, in the spectrum of **1** (Fig. 3, left panel), which is in agreement with the change in the oxidation state of Mo from Mo^I to Mo^{II} upon the formation of **1**. The IR spectrum of the starting complex $\{CpFe(CO)_2\}_2$ exhibits two split bands at 1756, 1771 cm^{-1} and 1936, 1956 cm^{-1}.[13] After the formation of **4**, these bands are shifted to higher frequencies (1942, 1961, and 2006 cm^{-1}), as shown in the central panel of Fig. 3. This result can be explained by a change in the oxidation state of iron from Fe^I to Fe^{II}. On the other hand, the CO stretching modes for $Ph_5CpRu(CO)_2Cl$, the dimer $\{CpMo(CO)_3\}_2$, and $Fe_3(CO)_{12}$ are shifted to lower frequencies upon the coordination of donor $[Sn^{II}Pc(3-)]^{\bullet-}$ units (Fig. 3, right panel), indicating the partial reduction of the metal centers (Tables S1–S3).

Crystal structures

The geometries and key structural parameters for $[Sn^{II}Pc(2-)]^0$ and coordination complexes and salts **1** and **3**–**8** are listed in Table 3, and the molecular structures of these units are shown in Fig. 4. Owing to their large sizes, the tin(II) atoms are displaced out of the 24-atom Pc plane by 1.22–1.27 Å for both the neutral $[Sn^{II}Pc(2-)]^0$ and $[Sn^{II}Pc(3-)]^{\bullet-}$ radical anions. As a result, the equatorial Sn–N(Pc) bonds noticeably elongate up to 2.26 Å (Table 3). The coordination of transition metals to the tin(II) atoms stabilizes the Sn–N(Pc) bonds, which is reflected in the reductions of both their lengths

and displacements of the tin atoms from the 24-atom Pc plane in all of the coordination complexes. The smallest displacement of 0.90 Å was observed in **4**, whereas the displacements of 1.01–1.13 Å were observed for other complexes. The shortest Sn–M bond lengths of 2.49–2.51 Å correspond to the coordination complexes with iron atoms (**4** and **5**), and the Sn–M bond lengths for the other metals are 2.55–2.56 Å for **7** (Rh), 2.64 Å for **8** (Ru), and 2.68–2.76 Å for **1** and **6** (Mo).

Table 3. Geometric parameters for $Sn^{II}Pc(2-)$, coordination complexes, and salts **1** and **3**–**8**.

Compound and number of crystallographically independent units; Characteristic features	Average bond lengths, Å				Displacement of atoms from the 24-atom Pc plane, Å		Geometry of the coordination unit with the transition metal		
	Sn-N(Pc)	N_{im}-C short/long	N_{pyr}-C	Sn-M	Sn	N_{pyr}	M-C(CO)	C≡O group	M-C($Cp^{(*)}$)
$[Sn^{II}Pc(2-)]$[14]	2.266(3)	-	-	-	1.275	0.107–0.200	-	-	-
{Cp*MoBr(CO)$_2$ $[Sn^{II}Pc(2-)]$} ·0.5$C_6H_4Cl_2$ (**1**), 1 unit; infinite chains of dimeric Pc	2.214(2)	1.340(3)	1.393(3)	2.7593(3)	1.131	0.077-0.183	1.982(4) Mo-Br 2.697(8)	1.162(2)	2.366(4)
{cryptand(Na^+)} $[Sn^{II}Pc(3-)]^{\bullet-}$ ·$C_6H_4Cl_2$ (**3**), 2 units; channel structure, isolated Pc	2.253(6) 2.258(6)	1.326(9)/ 1.334(9) 1.326(10)/ 1.327(10)	1.387(10) 1.381(10)	-	1.225 1.268	0.093-0.185 0.123-0.197	-	-	-
{cryptand(Na^+)} $\{CpFe(CO)_2[Sn^{II}Pc(4-)]\}^-$ ·1.5$C_6H_4Cl_2$ (**4**), 1 unit; channel structure	2.132(3)	1.294(4)/ 1.368(4)	1.396(4)	2.5087(5)	0.905	0.066-0.143	1.764(4)	1.146(4)	2.102(4)
{cryptand(Na^+)} $\{Fe(CO)_4[Sn^{II}Pc(3-)]^{\bullet-}\}$ ·1/3$C_6H_4Cl_2$ (**5**), 2 units; stacks of shifted Pc dimers	2.154(3) 2.164(3)	1.324(5)/ 1.336(5) 1.308(5)/ 1.347(5)	1.386(5) 1.386(5)	2.4947(6) 2.4947(9)	1.015 1.084	0.140-0.194 0.158-0.274	1.781(7) 1.772(8)	1.151(8) 1.144(8)	- -
{cryptand(Na^+)} $\{CpMo(CO)_2[(Sn^{II}Pc(2-)Sn^{II}Pc(3-)^{\bullet-}]\}$ ·3.5$C_6H_4Cl_2$ (**6**), 2 units	2.161(5) 2.159(5)	1.318(6)/ 1.334(7) 1.320(6)/ 1.343(7)	1.393(7) 1.386(8)	2.6876(6) 2.6855(6)	1.026 1.020	0.075-0.157 0.109-0.123	1.986(6)	1.158(5)	2.331(5)
{cryptand(Na^+)} $\{Cp^*RhCl_2[Sn^{II}Pc(3-)]^{\bullet-}\}$ ·$C_6H_4Cl_2$ (**7**), 2 units; chains through Cp^*RhCl_2	2.182(6) 2.183(6)	1.319(7)/ 1.338(7) 1.312(7)/ 1.339(7)	1.385(7) 1.388(.7)	2.5584(7) 2.5677(7)	1.090 1.093	0.102-0.174 0.104-0.204	Rh-Cl 2.400(2) 2.408(2)	- -	2.178(7) 2.170(7)
$\{Ph_5CpRu^{II}(CO)_2$ $[Sn^{II}Pc(3-)]\}$ (**8**), 1 unit; isolated Pc dimers	2.148(2)	1.316(3)/ 1.341(3)	1.389(3)	2.6486(3)	1.028	0.064-0.257	1.887(3)	1.139(3)	2.271(2)

In neutral $[Sn^{II}Pc(2-)]^0$, each of the eight pyrrolo-nitrogen to carbon (N_{pyr}–C) and imino-nitrogen to carbon (N_{im}–C) bonds in the Pc macrocycle has a different length (Table 3), and no alternation of these bonds was observed. The alternation of the N_{im}–C bonds did appear, however, after the reduction of the Pc macrocycle, because four of the bonds belonging to two oppositely located

isoindole units were elongated, and four other bonds were shortened. Bond alternation has also been observed for other complexes including metal phthalocyanine radical anions, $[MPc]^{\bullet-}$ (M = Cu^{II}, Ni^{II}, Sn^{II}, Pb^{II}, $Sn^{IV}Cl_2$, $Ti^{IV}O$, and $V^{IV}O$) in which the Pc macrocycle is reduced and explained by the partial disruption of the aromaticity of the Pc ligand.[8e] A similar tendency was observed for the coordination complexes discussed in this study. The starting compound $[Sn^{II}Pc(2-)]^0$ and complex **1** with the neutral $[Sn^{II}Pc(2-)]^0$ ligand did not exhibit the alternation of the N_{im}–C bonds, but such an alternation was observed for complexes **4**–**8** with negatively charged $Sn^{II}Pc$ ligands. The greatest difference between the short and long N_{im}–C bonds was observed in **4**, indicating that the partial

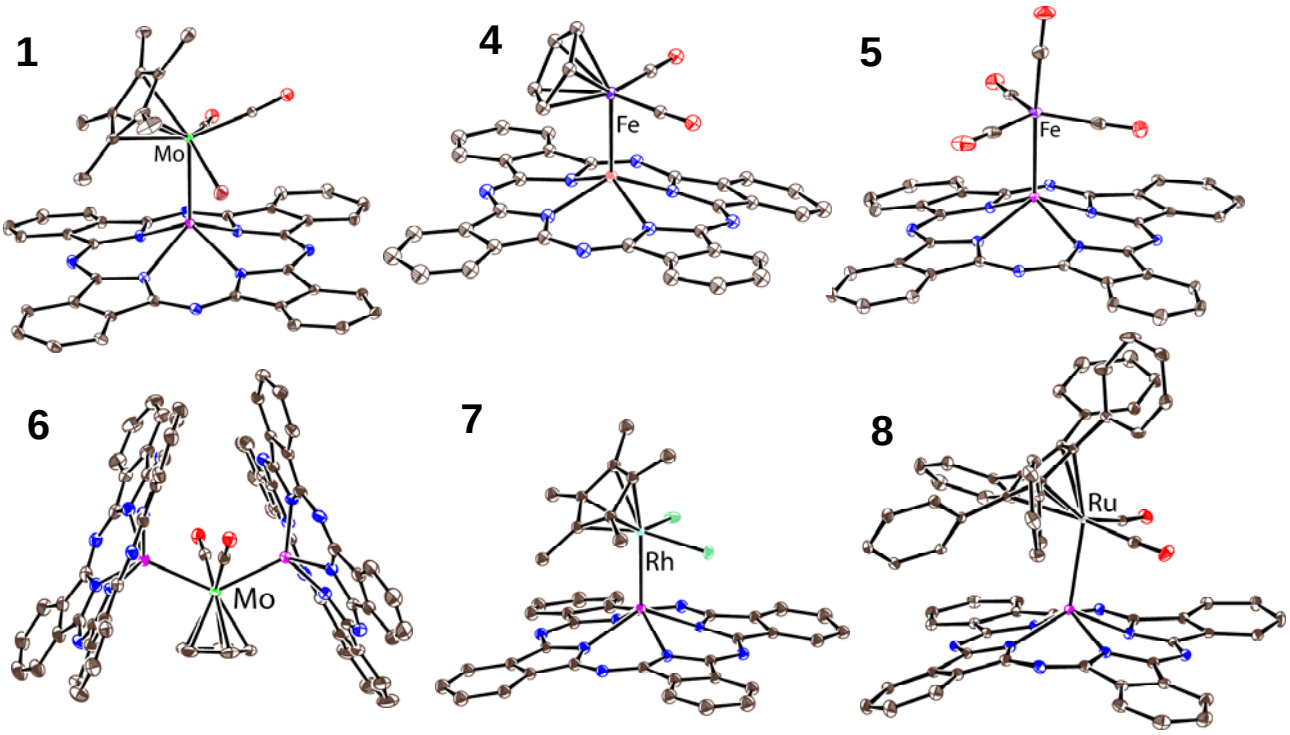

Figure 4. Molecular structures of coordination units (numbers are in accordance with Table 1: (**1**) Neutral $Cp^*MoBr(CO)_2[Sn^{II}Pc(2-)]$ species (carbonyl groups and Br anions are shown in one orientation), (**4**) $\{CpFe^{II}(CO)_2[Sn^{II}Pc(4-)]\}^-$ anions, (**5**) $\{Fe(CO)_4[Sn^{II}Pc(3-)]^{\bullet-}\}$ anions, (**6**) $\{CpMo(CO)_2[(Sn^{II}Pc(2-)(Sn^{II}Pc(3-)^{\bullet-}]\}$ anions, (**7**) $\{Cp^*RhCl_2[Sn^{II}Pc(3-)]^{\bullet-}\}$ anions, and (**8**) neutral $Ph_5CpRu(CO)_2[Sn^{II}Pc(3-)]$ units.

disruption of aromaticity is also a characteristic of the $[Sn^{II}Pc(4-)]^{2-}$ dianion (Table 3). The Pc macrocycles in **1** and **3**–**8** (Fig. 4) adopted concave conformations owing to the displacement of the tin(II) atoms from the 24-atom Pc plane. In some cases, a greater deviation of one of the four isoindole units from planarity was observed, which can be explained by the coordination of the bulky metal fragments, such as Cp^*RhCl_2 or $Ph_5CpRu(CO)_2$.

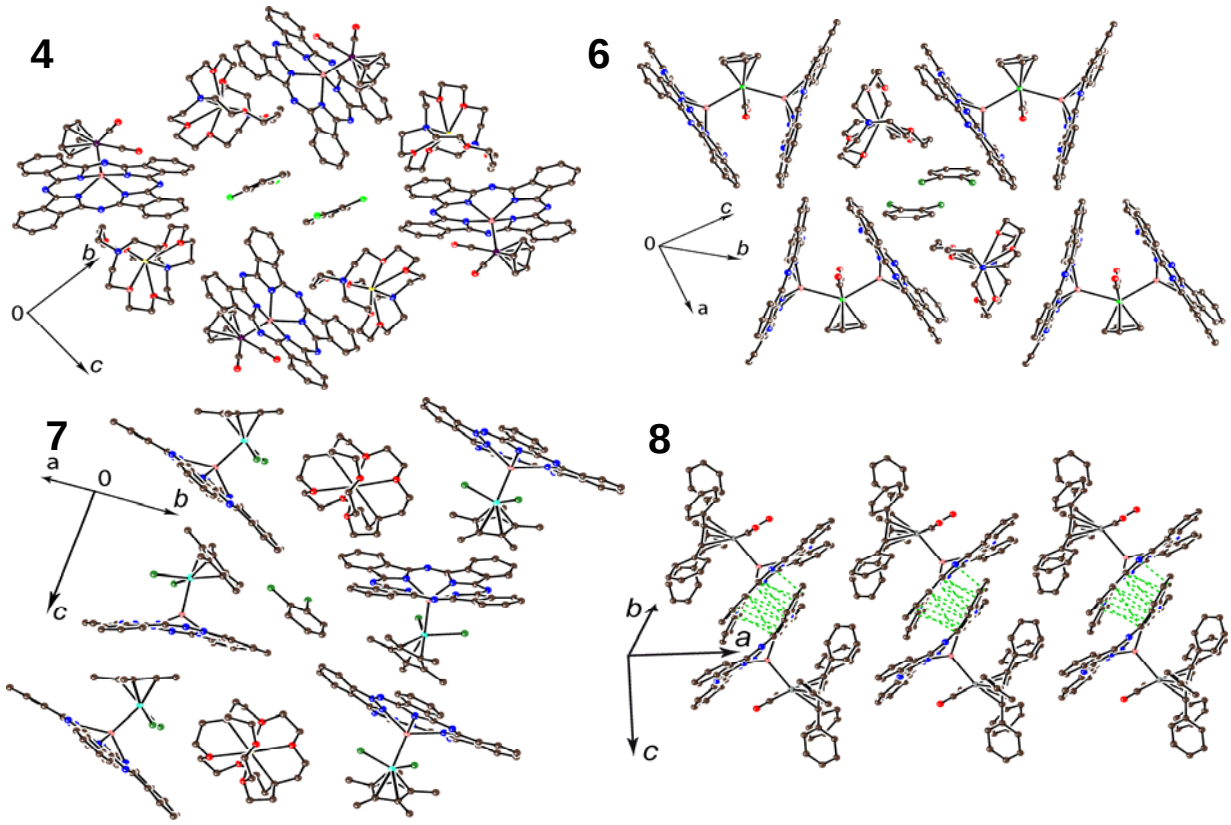

Figure 5. Crystal structures of compounds 4 and 6–8 (numbers are in accordance with Table 1): (**4**) channels formed by $\{CpFe(CO)_2[Sn^{II}Pc(4-)]\}^-$ anions and cryptand(Na^+) cations, (**6**) channels formed by four $\{CpMo(CO)_2[(Sn^{II}Pc(2-)[(Sn^{II}Pc(3-)^{\bullet-}]\}$ species, (**7**) chains of$\{Cp^*RhCl_2[Sn^{II}Pc(3-)]^{\bullet-}\}$, and (**8**) π-stacking dimers formed by $Ph_5CpRu(CO)_2[Sn^{II}Pc(3-)]$. Disordered parts are shown in their major orientations. Shortened van der Waals C, N…C, N contacts are shown by green dashed lines.

The crystal structures of **1** and **3**–**8** are shown in Figs. 5–6 and S9–S10 in the Supporting information. Salt **3** contains two types of channels formed by four $[Sn^{II}Pc(3-)]^{\bullet-}$ planes (Fig. S9). These channels are occupied by the cryptand(Na^+) cations or alternating cryptand(Na^+) and $C_6H_4Cl_2$ molecules. No π–π interactions between the $[Sn^{II}Pc(3-)]^{\bullet-}$ ligands are present in **3** owing to their perpendicular arrangement.

The structure of **4** contains channels formed by four {cryptand(Na^+)}{$CpFe^{II}(CO)_2[Sn^{II}Pc(4-)]^-$} units, and the cryptand(Na^+) cations are positioned in the vacancies formed by the concave Pc macrocycles. The channels are occupied by $C_6H_4Cl_2$ molecules (Fig. 5).

The large channels formed by four {$CpMo(CO)_2[Sn^{II}Pc(2-)Sn^{II}Pc(3-)^{\bullet-}]$} units in **6** are occupied by cryptand(Na^+) cations and $C_6H_4Cl_2$ (Fig. 5). As a result, these units are completely isolated.

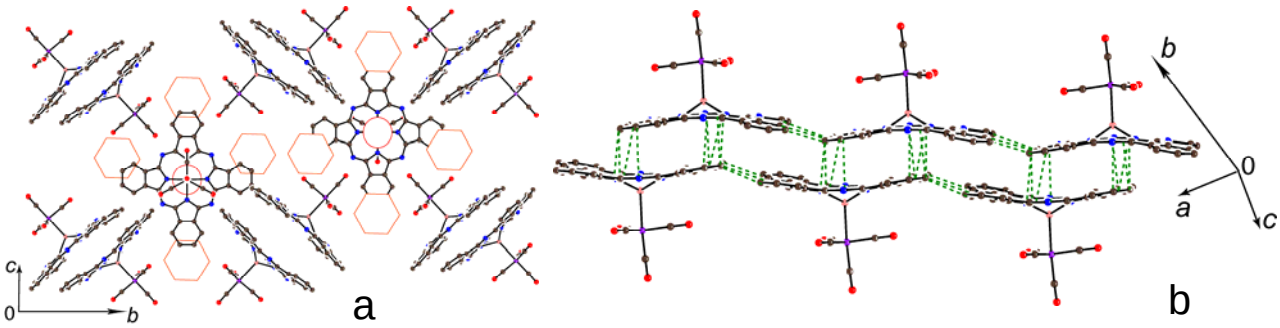

Figure 6. Crystal structure of {cryptand(Na^+)}{$Fe(CO)_4[Sn^{II}Pc(3-)]^{\bullet-}$}·(1/3)$C_6H_4Cl_2$ (**5**): (a) view along *a* axis. Cryptand(Na^+) cations and $C_6H_4Cl_2$ molecules are indicated by red hexagons and circles, respectively; (b) view of chain formed of π-stacking dimers; shortened vdW C,N…C,N contacts are indicated by green dashed lines.

Chains in which the Cp* ligand of one {$Cp^*RhCl_2[Sn^{II}Pc(3-)]^{\bullet-}$} is involved in π–π stacking interactions with the Pc ligand of an adjacent {$Cp^*RhCl_2[Sn^{II}Pc(3-)]^{\bullet-}$} are formed in **7** (Fig. 5). The angles between the planes of the Cp* ligands and the isoindole units are just 5.3° and 7.1°, indicating a nearly parallel arrangement, and the van der Waals (vdW) contacts between these

planes are on the boundary of vdW interactions (3.40–3.55 Å). The zigzag arrangement of the {Cp*RhCl$_2$[Sn^{II}Pc(3-)]$^{\bullet-}$} chains provides separate channels for cryptand(Na$^+$) and $C_6H_4Cl_2$ (Fig. 5).

The structure of **1** (Fig. S10a) contains the infinite chains of π–π stacking {Cp*Mo(Br)$_{0.82}$(CO)$_{1.78}$[Sn^{II}Pc(2−)]}$_2$ dimers. The interplanar distance in the dimers is 3.39 Å and allows the formation of several vdW C,N···C,N contacts between the phthalocyanines that range from 3.18 Å to 3.38 Å.

Complex **5** has an unusual structure. It contains phthalocyanine chains formed by π-stacking dimers with shifted Pc planes (Fig. 6b). The interplanar distance in the dimers is 3.28 Å, and the shortest vdW C, N···C,N contacts are longer than 3.38 Å. A second type of Fe(CO)$_4$[Sn^{II}Pc(3-)]$^{\bullet-}$ unit alternates with the cryptand(Na$^+$) cations and solvent $C_6H_4Cl_2$ molecules (indicated by red circles and hexagons, respectively, in Fig. 6a). As a result, the Pc planes of these coordination units are separated by a distance of 12.94 Å.

Isolated π−π stacking dimers are formed in **8** (Fig. 5). These dimers have the shortest interplanar distance among the dimers in all of the studied complexes (3.25 Å) and 17 short vdW C,N···C,N contacts ranging from 3.17 to 3.27 Å in length (indicated by the green dashed lines in Fig. 5).

Magnetic properties

Magnetic property data (superconducting quantum interference device (SQUID) and electron paramagnetic resonance (EPR)) for compounds **1**−**8** are listed in Table 4 and Figs. S11−S24 in the Supporting information. The main contributions to the magnetic susceptibilities of these complexes are made by the transition metals, which in some cases have spin and negatively charged Pc$^{\bullet3-}$ radical trianions that (according to previous studies) have S = 1/2 spin states.[8d-f, 15] The crystal structures of the obtained complexes can be separated into two categories: complexes with channels

Table 4. SQUID and EPR data for **1**–**8**.

Compound	Magnetic moment at 300 K (μ_B)	Weiss temperature (temp. interval)	EPR spectra Low temperature *g*-factor (linewidth, mT)	 RT *g*-factor (linewidth, mT)
1	-	-	250 K (very weak signal) 1.9979 (8.85 mT) 1.9991 (0.225 mT) (0.3% of broad signal)	
2	-	-	100 K Signal from Fe^{I} 1.9878 (51 mT), HFS, 6 lines with 8.156 mT splitting	
3	1.63	−7 (30–300 K)	60.3 K 2.0039 (0.555) 2.0013 (0.770) 1.9954 (1.706)	RT 2.0047 (0.543) 2.0026 (0.619) 1.9959 (1.750)
4	0.72	−3.4 (20–300 K)	Weak signals 9.3 K 4.154 (16.45) 4.294 (5.37) Fe 2.0034 (0.615) 1.9960(1.56) $Pc^{\bullet 3-}$	Weak signals RT 4.280 (8.07) Fe 2.0039 (0.406) $Pc^{\bullet 3-}$
5	1.75	−28.6(70–300 K)	6 K 1.9952 (5.95) 1.9788 (8.58)	275.6 K 1.9986 (1.51) 1.9818 (61)
6	2.51	−27.6(45–300 K)	29 K 1.9990 (1.48) 1.9744 (11.63) 1.9247 (50.98)	245 K 2.0014 (0.80) <0.1%
7	1.75	−7.7 (40–300 K)	60 K 1.9895 (13.40) 1.9516 (12.73) 1.9197 (20.27)	160.5 K 1.6629 (141.04) 1.9874 (67.47)
8	1.66	Curie impurity (3%), $J/k_B = -183$ K	28.7 K 2.0035 (0.604) 1.9995(0.904) 1.9992 (1.864)	RT absent

occupied by the cryptand(Na^+) cations and/or solvent $C_6H_4Cl_2$ molecules have no π−π interactions between the Pc macrocycles, and as a result no essential magnetic coupling is possible. Complexes in which the Pc macrocycles form π-stacking dimers have π−π interactions between the Pc macrocycles and sufficiently strong antiferromagnetic spin coupling can be realized. Complex **1** consists of diamagnetic $[Sn^{II}Pc(2-)]^0$ and Mo atoms. Mo atoms with formal +1 charges are

paramagnetic.[16] However, the coordination of $\{Cp^*Mo^{I}(CO)_2\}_2$ to $[Sn^{IV}Br_2Pc(3-)]^{\bullet-}$ is accompanied by oxidation of Mo^{I} to Mo^{II} and the formation of $Cp^*Mo^{II}Br(CO)_2$, which should be EPR-silent. Indeed, no EPR signal from Mo^{I} was observed in the spectrum of **1** (EPR active $CpMo^{I}(CO)_2$ species coordinated to fullerenes or carbon nanotubes have *g*-factors ranging from 1.975 to 2.029[16b]). A weak EPR signal with g = 1.9979 and a linewidth (ΔH) of 8.85 mT (Fig. S13) with an intensity less than 2% of the spins based on the total quantity of $Sn^{II}Pc(2-)$ was most likely due to an $[Sn^{II}Pc(3-)]^{\bullet-}$ impurity.

Complex **2** contains diamagnetic $[Sn^{II}Pc(2-)]^0$ and paramagnetic Fe^{I} with a d^7 electron configuration. Not surprisingly, **2** manifested a very broad intense EPR signal with g = 1.9878 and ΔH = 51 mT at 100 K (Fig. 7a). Because the hyperfine structure of this signal consisted of 6 lines with an average splitting of 8.156 mT (Fig. 7a), the signal was attributed to Fe^{I} with an S = 1/2 spin state. The Fe^{I} in $[Fe^{I}Pc(2-)]^-$ anions has a similar electronic configuration.[8a, b]

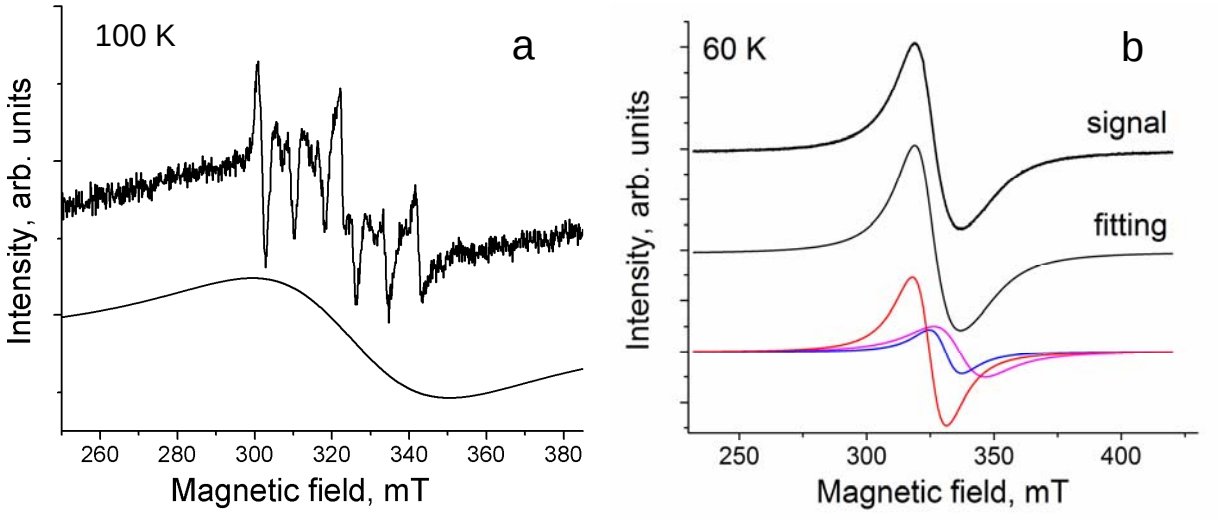

Figure 7. (a) EPR signal for polycrystalline **2** at 100 K. Fitting of broad signal by one Lorentzian line is also shown; (b) EPR signal for polycrystalline **7** at 60 K. Fitting of signal by three Lorentzian lines is also shown.

The magnetic properties of an individual $[Sn^{II}Pc(3-)]^{\bullet-}$ ligand were studied in **3**. Its magnetic moment was found to be 1.63 μ_B at 300 K (Fig. S11a). This value is close to that calculated for a system with one non-interacting S = 1/2 spin per formula unit (μ_{eff} = 1.73 μ_B). The temperature dependence of the reciprocal magnetic susceptibility of **3** was linear from 30 K to 300 K, and the Weiss temperature was calculated to be −7 K (Fig. S11b). This value indicates rather weak antiferromagnetic spin coupling in **3** due to the absence of π−π interactions between the Pc macrocycles. The salt also exhibited an asymmetric EPR signal at room temperature (RT) that was fitted by three Lorentzian lines with g_1 = 2.0047 (ΔH = 0.543 mT), g_2 = 2.0026 (ΔH = 0.619 mT), and g_3 = 1.9959 (ΔH = 1.750 mT) (Fig. S12b). In fact, this three-component signal was observed down to 4 K with close g-factor values and only slight changes in the linewidths (Figs. S12b and S12c). Previously studied salts containing $[Sn^{II}Pc(3-)]^{\bullet-}$ also exhibited very asymmetric signals, but most of the components were essentially broader at low temperatures[8e].

It is thought that charge transfer from $CpFe^{I}(CO)_2$ to $[Sn^{II}Pc(3-)]^{\bullet-}$ takes place in **4**, producing diamagnetic $[Sn^{II}Pc(4-)]^{2-}$ dianions and, correspondingly, $[CpFe^{II}(CO)_2]^{+}$ cations. Indeed, without such charge transfer, the complex would have contributions from two S = 1/2 spins per formula unit from $CpFe^{I}(CO)_2$ and $[Sn^{II}Pc(3-)]^{\bullet-}$, with an expected magnetic moment of ~2.45 μ_B. The lower magnetic moment of 0.72 μ_B at 300 K (Fig. S14a) supports the occurrence of charge transfer. The estimated Weiss temperature of −3.4 K (Fig. S14b) also indicates the absence of magnetic spin coupling in **4**. The complex exhibited two sets of weak EPR signals (Fig. S15) that may originate from $Pc^{\bullet3-}$ and iron-containing impurities (Table 4).

Complex **5** with paramagnetic $[Sn^{II}Pc(3-)]^{\bullet-}$ and diamagnetic $Fe^{0}(CO)_4$ groups was found to have a magnetic moment of 1.75 μ_B at 300 K (a contribution of one S = 1/2 spin per formula unit) (Fig. S16a); its Weiss temperature of −28.6 K (Fig. S16b) indicates sufficiently strong antiferromagnetic

spin coupling. Because 2/3 of the paramagnetic $[Sn^{II}Pc(3-)]^{\bullet-}$ species in **5** are packed in π–π stacking dimers, magnetic coupling can be realized in these dimers. The complex manifested an asymmetric EPR signal at 270 K that was fitted by two lines: a narrow line with g_1 = 1.9986 (ΔH = 1.51 mT) and a very broad line with g_2 = 1.9818 (ΔH = 61 mT). Narrowing of the broad line was observed only below 50 K (Figs. S17 and S18). These lines are attributed to $[Sn^{II}Pc(3-)]^{\bullet-}$.

Isolated $CpMo^{I}(CO)_2[Sn^{II}Pc(2-)Sn^{II}Pc(3-)^{\bullet-}]$ units are formed in **6**. One of the two $Sn^{II}Pc$ ligands is negatively charged and has an S = 1/2 spin state. The $CpMo^{I}(CO)_2$ units are also paramagnetic, because Mo^{I} has a d^5 electron configuration. This behavior differs from that of anionic $(PPN^+)\{CpMo(CO)_2(\eta^2\text{-}C_{60(70)})\}^-$ (PPN^+ = bis(triphenylphosphoranylidene)ammonium cation) complexes, in which the fullerene$^{\bullet-}$ radical anions reduce $CpMo^{I}(CO)_2$ to form diamagnetic $C_{60(70)}{}^0$ and $CpMo^{0}(CO)_2$.[17] The magnetic moment of **6** was determined to be 2.51 μ_B at 300 K (Fig. S19a), which corresponds to a contribution of two S = 1/2 spins per formula unit. Therefore, both the $[Sn^{II}Pc(3-)]^{\bullet-}$ and $CpMo^{I}(CO)_2$ species with S = 1/2 spin states contribute to the magnetic moment. The calculated value for a system of two non-interacting S =1/2 spins is 2.45 μ_B. The Weiss temperature of −27.6 K for **6** was estimated in the range from 45 K to 300 K (Fig. S19b) and indicates sufficiently strong antiferromagnetic spin coupling in $CpMo^{I}(CO)_2[Sn^{II}Pc(2-)Sn^{II}Pc(3-)^{\bullet-}]$, likely because two paramagnetic species are separated by only one diamagnetic tin(II) atom. The EPR signal for **6** was observed only below 100 K and was approximated well by three Lorentzian lines with g_1 = 1.9990 (ΔH = 1.48 mT), g_2 = 1.9744 (ΔH = 11.63 mT), and g_3 = 1.9247 (ΔH = 50.98 mT) at 29 K (Fig. S20 shows the EPR signal at 19 K). A narrow component that was less than 0.2% of the two broader components was attributed to impurities, while the two broad components were assigned to $[Sn^{II}Pc(3-)]^{\bullet-}$, but a contribution by $CpMo^{I}(CO)_2$ to this signal is also possible, given that EPR active $CpMo^{I}(CO)_2$ species coordinated to fullerenes or carbon nanotubes have g-factors

ranging from 1.975 to 2.029.[14b] Both broad signals broadened even further as the temperature increased and could not be observed above 100 K, whereas the narrower component was detected even at RT (Fig. S21).

Complex **7** with $[Sn^{II}Pc(3-)]^{\bullet-}$ and diamagnetic $Cp^*Rh^{III}Cl_2$ exhibited behaviors very similar to those of **5**. The magnetic moment of **7** was found to be 1.75 μ_B at 300 K (Fig. S22a) and corresponds to the contribution of one $S = 1/2$ spin. The Weiss temperature was estimated to be −7.7 K (Fig. S22b). The $Cp^*Rh^{III}Cl_2[Sn^{II}Pc(3-)^{\bullet-}]$ anions form chains via π−π interactions of the Cp* ligands with one of four isoindole units of Pc. Nevertheless, any magnetic coupling between $[Sn^{II}Pc(3-)]^{\bullet-}$ is ineffectively transferred in these chains due to the diamagnetism of $Cp^*Rh^{III}Cl_2$. The EPR signal was approximated by three broad lines below 60 K with $g_1 = 1.9895$ ($\Delta H = 13.40$), g_2 =

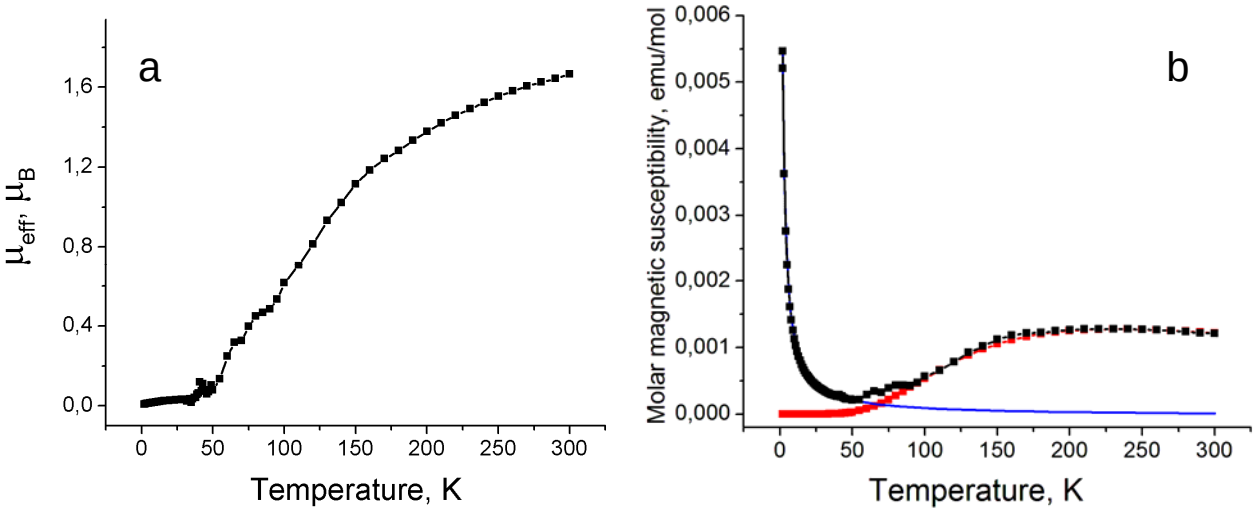

Figure 8. Temperature dependences of (a) effective magnetic moment and (b) molar magnetic susceptibility for polycrystalline **8**. Dependence in right panel was approximated by two contributions: (blue curve) Curie impurities (approximately 3% of spins based on the total quantity of $[Sn^{II}Pc(3-)]^{\bullet-}$) and (red curve) isolated pairs of antiferromagnetically interacting spins[16] with J/k_B = −183 K (approximated by Heisenberg model).

1.9516 (ΔH = 12.73 mT), and g_3 = 1.9197 (ΔH = 20.27 mT) at 60 K (Fig. 7b). These lines are significantly broadened above 100 K, and no signals were detected above 200 K (Fig. S23, Table 4).

Compound **8** is formally neutral. However, it contains negatively charged $[Sn^{II}Pc(3-)]^{\bullet-}$ and Ph_5Cp^- ligands for Ru. Therefore, Ru has a +2 oxidation state with a d^6 electron configuration and can potentially be diamagnetic (S = 0) or in an intermediate (S = 1) or high-spin states (S = 2). The magnetic moment for **8** was found to be 1.66 μ_B at 300 K (Fig. 8a) and is close to the value (1.73 μ_B) calculated for a system with one non-interacting S = 1/2 spin. It can thus be concluded that Ru adopts a diamagnetic S = 0 spin state in this compound. The molar magnetic susceptibility of **8** reached a maximum at approximately 200 K and then decreased at lower temperatures. The magnetic moment also decreased, even below 300 K, and never reached 1.73 μ_B, even at 300 K (Fig. 8). These results are attributed to very strong antiferromagnetic spin coupling in **8**. The molar magnetic susceptibility increased below 50 K due to manifestation of the Curie tail. The observed temperature dependence of the molar magnetic susceptibility can be presented as the sum of two contributions. One contribution is described by the Heisenberg model for the isolated pairs of antiferromagnetically interacting spins[18] with a magnetic exchange interaction of J/k_B = −183 K (red curve in Fig. 8b). The other originates from paramagnetic impurities (approximately 3% of the spins from the total amount of $[Sn^{II}Pc(3-)]^{\bullet-}$). This behavior was approximated well using the Curie−Weiss law with a Weiss temperature close to −1 K (blue curve in Fig. 8b). Complex **8** manifested a weak asymmetric EPR signal below 100 K (Figs. S24, Table 4) that most likely is due to the Curie impurities. It is assumed that strong magnetic coupling observed in **8** is realized within magnetically isolated π−π stacking dimers with short interplanar distances and multiple vdW C,N···C,N contacts. Previously, we found that the antiferromagnetic coupling in π−π stacking

$\{[Ti^{IV}OPc(3-)]^{\bullet-}\}_2$ dimers is sufficiently strong to cause the compound to fall into the diamagnetic state below 150 K.[8e]

Calculations

To examine the electronic structures of the $\{CpFe(CO)_2(SnPc)\}^-$ anion, $Ph_5CpRu(CO)_2(SnPc)$ monomer, and $[Ph_5CpRu(CO)_2(SnPc)]_2$ dimer, theoretical analyses using density functional theory (DFT) were performed at the M11/cc-pVTZ(-PP)/cc-pVDZ level of theory.[19] For the singlet, triplet, and quintet states in the $\{CpFe(CO)_2(SnPc)\}^-$ anion, the doublet and quartet states in the

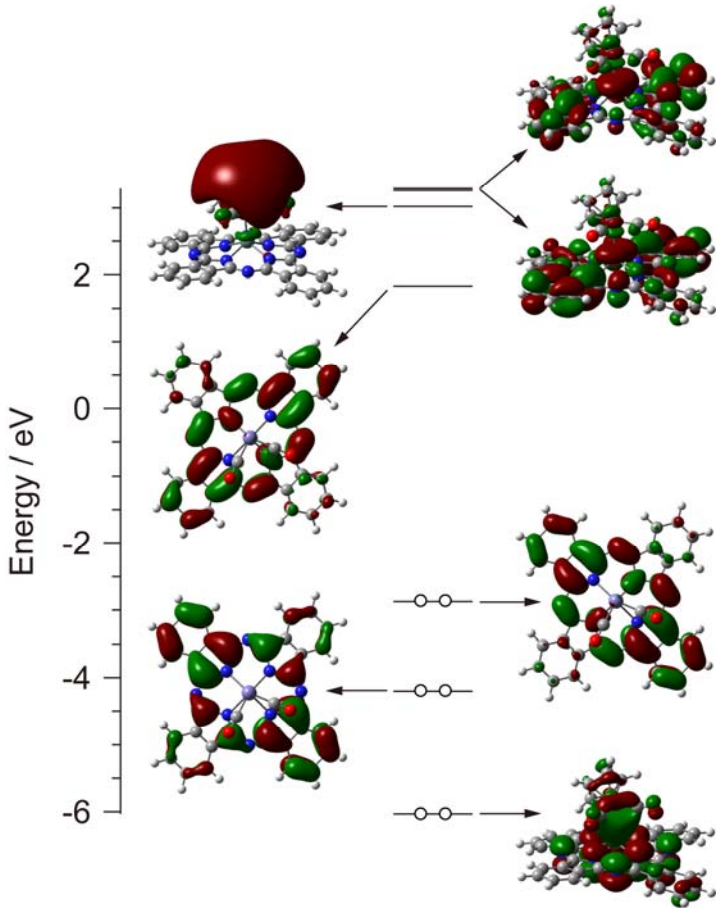

Figure 9. Energy diagram for the frontier Kohn−Sham orbitals of ^1A state in $[CpFe(CO)_2(SnPc)]^-$ anion calculated at the RM11/cc-pVTZ(-PP)/cc-pVDZ level of theory. For clarity, cyclopentadienyl ligand is omitted in HO-1, HO, and LU orbitals.

$Ph_5CpRu(CO)_2(SnPc)$ monomer, and the singlet and triplet states in the $[Ph_5CpRu(CO)_2(SnPc)]_2$ dimer, partial optimizations only for hydrogen atoms were completed using the X-ray structural data as the initial structures. The total and relative energies and $<S^2>$ values, the Mulliken and natural charges, and the Wiberg bond indices are summarized in Table S6, S7, and S8, respectively.

The closed-shell singlet state in the $\{CpFe(CO)_2(SnPc)\}^-$ anion is more stable in energy by 10630 K and 36899 K, respectively, than the corresponding triplet and quintet states, supporting the diamagnetic nature of **4**. Therefore, the observed magnetic moment and weak EPR signals of **4** appear to originate from paramagnetic impurities. The energy diagram for the frontier Kohn−Sham orbitals of the singlet state in the $\{CpFe(CO)_2(SnPc)\}^-$ anion is shown in Fig. 9. The highest occupied and lowest unoccupied molecular orbitals (HOMO and LUMO) stem from the doubly degenerated LUMO of the D_{4h} symmetric phthalocyaninate dianion (Pc^{2-}) (where the Pc ligand in **4** can be regarded as a closed shell Pc^{4-} tetraanion) and the (HO−1)MO from the HOMO of Pc^{2-}, respectively. From the electrostatic potential map shown in Fig. S25, it can be seen that the isoindole moieties over which the LUMO spreads are more negatively charged than those that are not affected. The (HO−2)MO and nearly degenerate (LU+2) and (LU+3)MOs are the bonding and antibonding orbitals between the Fe and Sn atoms, respectively. The Wiberg bond index for Fe−Sn bond was determined to be 0.641 (Table S8), and the Pc ligand had the largest negative natural charge of −2.822 (Table S7). In order to confirm the bond alternation of phthalocyanine moiety observed by X-ray structural analysis of **4**, full geometry optimization on the $[CpFe(CO)_2(SnPc)]^-$ anion was carried out at the RM11/cc-pVTZ(-PP)/cc-pVDZ level of theory. The calculated bond lengths and electrostatic potential map are shown in Table S9 and Figs. S25 and S26. The calculated bond lengths agree rather well with the experiment ones, indicating the high reliability of present DFT calculation. Although the phthalocyanine moiety in $[SnPc(2-)]^0$ is a 18 π-electronic system with aromaticity, the two-electron-reduction makes the phthalocyanine moiety a 20 π-electronic system to

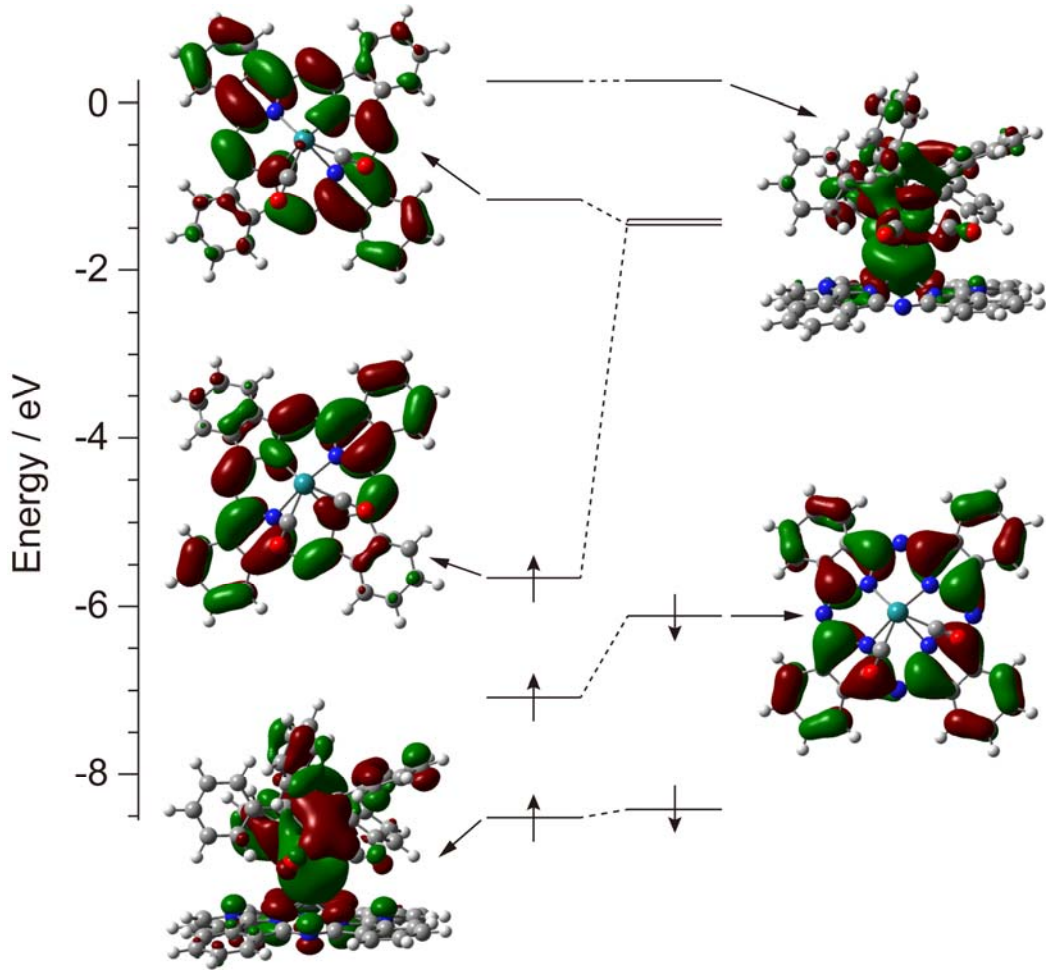

Figure 10. Energy diagram for frontier Kohn−Sham orbitals of ^2A state in $Ph_5CpRu(CO)_2(SnPc)$ monomer calculated at the UM11/cc-pVTZ-PP/cc-pVDZ level of theory. For clarity, the pentaphenylcyclopentadienyl ligand is omitted in α-LU, α-HO, and β-HO orbitals.

induce anti-aromaticity (Figure S27). The Pc moiety in the $[CpFe(CO)_2(SnPc)]^-$ anion may be deformed to the boat shape to get away from anti-aromatic character, which implies that anti-aromaticity would potentially come back when the Pc moiety gets the planarity by external stimuli such as pressure, light, and temperature.

The doublet state in the $Ph_5CpRu(CO)_2(SnPc)$ monomer and open-shell broken-symmetry singlet state in the $[Ph_5CpRu(CO)_2(SnPc)]_2$ dimer are more stable in energy than the corresponding quartet and triplet states, respectively. For the $[Ph_5CpRu(CO)_2(SnPc)]_2$ dimer, the estimated intermolecular

antiferromagnetic interaction was calculated to be J = −292 K, supporting the observed antiferromagnetic behavior with a value for J = −183 K between the S = 1/2 spins in **8**. The energy diagrams for the frontier Kohn−Sham orbitals of the doublet state in the $Ph_5CpRu(CO)_2(SnPc)$ monomer and the broken-symmetry singlet state in the $[Ph_5CpRu(CO)_2(SnPc)]_2$ dimer are shown in Figs. 10 and S28, respectively. The electronic structure of $Ph_5CpRu(CO)_2(SnPc)$ resembles that of the $\{CpFe(CO)_2(SnPc)\}^-$ anion. The singly occupied molecular orbital (SOMO) and LUMO stem from the doubly degenerate LUMO of the D_{4h} symmetric Pc^{2-}, where the Pc ligand in **8** can be regarded as an open-shell $Pc^{\bullet 3-}$ radical trianion, and the HOMO from the HOMO of Pc^{2-}. The (HO−1) and (LU+1)MOs are the bonding and antibonding orbitals between the Ru and Sn atoms, respectively. The electrostatic potential map shown in Fig. S29 is similar to that for the $\{CpFe(CO)_2(SnPc)\}^-$ anion.

The electronic structure of the broken-symmetry singlet state in the $[Ph_5CpRu(CO)_2(SnPc)]_2$ dimer inherits that of the doublet state in the $Ph_5CpRu(CO)_2(SnPc)$ monomer, and the two SOMOs (α- and β-HOMOs) providing the magnetic properties originate from the SOMO of the $Ph_5CpRu(CO)_2(SnPc)$ monomer (Fig. S28). The spin density distribution of the doublet state in the $Ph_5CpRu(CO)_2(SnPc)$ monomer and broken-symmetry singlet state in the $[Ph_5CpRu(CO)_2(SnPc)]_2$ dimer are shown in Figs. S30 and S31, respectively. It can be seen that they spread over the Pc ligand. This result was also confirmed by evaluating the Mulliken and natural spin densities of nearly one spin on a Pc ligand (Table S7). The present DFT calculations reveal that the magnetic properties of **8** derive from the π-radical spins on the Pc ligand. The Wiberg bond indices for the Ru−Sn bond in the $Ph_5CpRu(CO)_2(SnPc)$ monomer and $[Ph_5CpRu(CO)_2(SnPc)]_2$ dimer were found to be 0.724 and 0.716, respectively (Table S8), and the Pc ligands in the $Ph_5CpRu(CO)_2(SnPc)$ monomer and $[Ph_5CpRu(CO)_2(SnPc)]_2$ dimer had largest negative natural charges of −1.897 and −1.952 (Table S7).

Since the differences in the calculated charge and spin densities and Wiberg bond indices for the $Ph_5CpRu(CO)_2(SnPc)$ monomer and $[Ph_5CpRu(CO)_2(SnPc)]_2$ dimer were small, the results for the $Ph_5CpRu(CO)_2(SnPc)$ monomer were further investigated. Specifically, the natural charges of the $[CpFe(CO)_2(SnPc)]^-$ anion and $Ph_5CpRu(CO)_2(SnPc)$ monomer were compared (Table S7). Except for the Pc ligands in the $[CpFe(CO)_2(SnPc)]^-$ anion and $Ph_5CpRu(CO)_2(SnPc)$ monomer, the natural charges on the corresponding moieties resembled one another, indicating that the Fe and Ru atoms, Cp and Ph_5Cp ligands, CO ligands, and Sn atoms in **4** and **8** have nearly the same charges. Therefore, on a formal charge basis, if the Ph_5Cp ligand has a charge of −1, the Cp ligand should also have a charge of −1, and if the Ru atom has a charge of +2, the Fe ligand should also have a charge of +2. Note that the absolute values of the natural charges do not exactly match those of the formal charges. However, the similar charges (except for the Pc ligands) and similar Wiberg bond indices for the Fe−Sn and Ru−Sn bonds in Tables S7 and S8 indicate that the electronic structures of the $[CpFe(CO)_2(SnPc)]^-$ anion and $Ph_5CpRu(CO)_2(SnPc)$ monomer are roughly the same, except for the Pc ligand. On the other hand, the Pc ligand in the $[CpFe(CO)_2(SnPc)]^-$ anion has a larger negative charge by approximately one electron than that in the $Ph_5CpRu(CO)_2(SnPc)$ monomer (−2.822 vs. −1.897 in Table S7). It can therefore be concluded that the Pc ligand is in a tetraanionic state, such as $\{CpFe^{II}(CO)_2[Sn^{II}Pc(4-)]^{2-}\}^-$, because the optical and magnetic properties and frontier orbital picture indicate an electronic structure of $Ph_5CpRu^{II}(CO)_2[Sn^{II}Pc(3-)]^{\bullet-}$ on a formal charge basis. In other words, complex **4** is generated as the result of charge transfer from $CpFe^{I}(CO)_2$ to $[Sn^{II}Pc(3-)]^{\bullet-}$ to form $\{CpFe^{II}(CO)_2[Sn^{II}Pc(4-)]^{2-}\}^-$ dianions.

CONCLUSION

New approaches for obtaining crystalline transition metal complexes with neutral tin(II) phthalocyanine and tin(II) phthalocyanine radical anions and dianions were described. The ability of tin(II) atoms to form stable Sn−M bonds with transition metals (Mo, Fe, Rh, and Ru) was utilized.

Other metals can also form such bonds (In, Ga, Bi, and others), and we plan to study these complexes in the future. In all cases except $CpFe(CO)_2$, the negative charge and spin on the coordinated $[Sn^{II}Pc(3-)]^{\bullet-}$ radical anions were preserved, and the anions acted as anionic paramagnetic ligands for the transition metals. In the coordination complex of $CpFe^{I}(CO)_2$ with $[Sn^{II}Pc(3-)]^{\bullet-}$, unusual charge transfer was observed, along with the formation of $\{CpFe^{II}(CO)_2\}^{+}$ cations and $[Sn^{II}Pc(4-)]^{2-}$ dianions. This new approach thus provides a potential method for developing magnetic and conducting assemblies based on metal phthalocyanines and transition metals with significant variability: neutral, monoanionic, and even dianionic tin(II) phthalocyanines can be obtained. It was also found that the formally neutral $Ph_5CpRu^{II}(CO)_2[Sn^{II}Pc]$ molecule contains $[Sn^{II}Pc(3-)]^{\bullet-}$ radical anions. This compound is of a special interest because these molecules manifest strong magnetic spin coupling.

EXPERIMENTAL

Materials

Tin(II) phthalocyanine ($Sn^{II}Pc$), tin(IV) phthalocyanine dichloride ($Sn^{IV}Cl_2Pc$), and (cyclopentadienyl iron(I) dicarbonyl $\{CpFe(CO)_2\}_2$ dimer were purchased from TCI. Molybdenum(I) cyclopentadienyl tricarbonyl $\{CpMo(CO)_3\}_2$ dimer, pentamethylcyclopentadienyl rhodium(III) dichloride $\{Cp^*RhCl_2\}_2$ dimer, pentaphenylcyclopentadienyl ruthenium(II) dicarbonyl chloride $Ph_5CpRu(CO)_2Cl$, and tetrabutylammonium bromide (Bu_4NBr, 99%) were purchased from Aldrich. Cryptand[2,2,2] and triiron dodecacarbonyl $Fe_3(CO)_{12}$ (99%) were purchased from Acros. Pentamethylcyclopentadienyl molybdenum(I) dicarbonyl $\{Cp^*Mo(CO)_2\}_2$ dimer was purchased from Strem. Sodium fluorenone ketyl was obtained as described.[20] Solvents were purified under an Ar atmosphere. *Ortho*-dichlorobenzene ($C_6H_4Cl_2$) was distilled over CaH_2 under reduced pressure, and hexane was distilled over Na/benzophenone. Compounds **1–8** were synthesized and stored in an MBraun 150B-G glove box with a controlled atmosphere containing less than 1 ppm each of water

and oxygen. Solvents were degassed and stored in the glove box, and the KBr pellets used for the IR and UV−visible−NIR analyses were prepared in the glove box. EPR and SQUID measurements were performed on polycrystalline samples of **1**–**8** sealed in 2 mm quarz tubes at ambient pressure.

Synthesis

Crystals of **1**–**8** were obtained using a diffusion technique. A reaction mixture in *o*-dichlorobenzene was filtered into a 1.8-cm-diameter, 50 mL glass tube with a ground glass plug, and then 30 mL of hexane was layered over the solution. Slow mixing of the *o*-dichlorobenzene solution with hexane resulted in precipitation of crystals over 1−2 months. The solvent was then decanted from the crystals, and they were washed with hexane. The compositions of the obtained compounds were determined via X-ray diffraction analysis of a single crystal of each (see Supporting information for X-ray diffraction data). For each compound, several crystals from one synthesis were found to consist of a single crystalline phase. The compositions of the neutral coordination complexes were confirmed using elemental analysis. Due to the high air sensitivity of compound **3**–**8**, elemental analysis could not be used to determine the composition, because the complexes reacted with oxygen in the air before the quantitative oxidation procedure could be performed.

$Cp^*MoBr(CO)_2[Sn^{II}Pc(2-)]\cdot 0.5C_6H_4Cl_2$ (**1**) was obtained via the reduction of $Sn^{IV}Cl_2Pc$ (29.3 mg, 0.042 mmol) using a slight excess of sodium fluorenone ketyl (11 mg, 0.054 mmol) in the presence of excess Bu_4NBr (30 mg, 0.092 mmol) in *o*-dichlorobenzene (16 ml). The reaction was performed for 2 h at 100 °C. The resulting deep blue solution containing the TBA^+ salt of $[Sn^{IV}Br_2Pc(3-)]^{\bullet-}$ was filtered into a flask containing one equivalent of $\{Cp^*Mo(CO)_2\}_2$ dimer (24 mg, 0.042 mmol), and the solution was stirred for 1 d at 80 °C to produce a green solution. The solution was cooled to room temperature and then filtered into a tube for diffusion. Black prisms were obtained in 32% yield. The composition of **1** was confirmed via elemental analysis: Anal. Calcd for $C_{47}H_{33}BrClMoN_8O_2Sn$, M_r = 1072: C 52.66, H 3.08, N 10.45; Found: C 53.02, H 2.96, N 10.38. The

introduction of Br anions linked to Mo atoms was justified by the length of the Mo-Br bond of 2.697(8) Å in **1**, which is characteristic of the length of the Mo-Br bonds in the $CpMo(CO)_2$-containing compounds (~2.63−2.67 Å).[11] Mo−Cl bonds are noticeably shorter (~2.47−2.54 Å).[11c, 12]

$CpFe(CO)_2[Sn^{II}Pc(2-)]\cdot 2C_6H_4Cl_2$ (**2**) was obtained via the reduction of $Sn^{IV}Cl_2Pc$ (29.3 mg, 0.042 mmol) using a slight excess of sodium fluorenone ketyl (11 mg, 0.054 mmol) in the presence of one equivalent of cryptand (16 mg, 0.042 mmol) in *o*-dichlorobenzene (16 ml). The reaction was performed for 2 h at 100 °C. The resulting deep blue solution containing $\{cryptand(Na^+)\}[Sn^{IV}Cl_2Pc(3-)]^{\bullet-}$ was filtered into a flask containing excess $\{CpFe(CO)_2\}_2$ dimer (24 mg, 0.068 mmol), and the resultant solution was stirred for 1 d at 80 °C to produce a greenish-blue solution. This solution was subsequently cooled to RT and then filtered into a tube for diffusion. Black rhombs with a characteristic copper luster were obtained in 58% yield. The composition of **2** was determined via elemental analysis: Anal. Calcd for $C_{51}H_{24}Cl_4FeN_8O_2Sn$, M_r = 1097: C 55.80, H 2.19, N 10.21, Cl 12.94; Found: C 55.96, H 2.34, N 10.14, Cl 12.32. All measurements were performed on freshly isolated crystals.

$\{Cryptand(Na^+)\}[Sn^{II}Pc(3-)]^{\bullet-}\cdot C_6H_4Cl_2$ (**3**) was obtained via the reduction of $Sn^{II}Pc$ (26.4 mg, 0.042 mmol) with a slight excess of sodium fluorenone ketyl (11 mg, 0.054 mmol) in the presence of one equivalent of cryptand (16 mg, 0.042 mmol) in *o*-dichlorobenzene (16 ml) for 2 h at 100 °C. The resulting deep blue solution was cooled to RT and then filtered into a tube for diffusion. Black parallelepipeds of **3** with a characteristic copper luster were obtained in 74% yield.

$\{Cryptand(Na^+)\}\{CpFe(CO)_2[Sn^{II}Pc(4-)]\}^{-}\cdot C_6H_4Cl_2$ (**4**) was obtained via the reduction of $Sn^{II}Pc$ (26.4 mg, 0.042 mmol) with a slight excess of sodium fluorenone ketyl (11 mg, 0.054 mmol) in the presence of one equivalent of cryptand (16 mg, 0.042 mmol) in *o*-dichlorobenzene (16 ml). The resulting deep blue solution was filtered into a flask with containing excess $\{CpFe(CO)_2\}_2$ dimer (24 mg, 0.068 mmol), and the resultant solution was stirred for 1 d at 80 °C to produce a deep violet

solution. This solution was subsequently cooled to RT and then filtered into a tube for diffusion. Black prisms with a characteristic copper luster were obtained in 72% yield.

To prepare the crystalline $\{cryptand(Na^+)\}\{Fe(CO)_4[Sn^{II}Pc(3-)]^{\bullet-}\}\cdot(1/3)C_6H_4Cl_2$ (**5**), $\{cryptand(Na^+)\}\{CpMo(CO)_2[(Sn^{II}Pc)_2]^{\bullet-}\}\cdot 3.5C_6H_4Cl_2$ (**6**), $\{cryptand(Na^+)\}\{Cp^*RhCl_2[Sn^{II}Pc(3-)]^{\bullet-}\}\cdot C_6H_4Cl_2$ (**7**), and $Ph_5CpRu^{II}(CO)_2[Sn^{II}Pc(3-)]$ (**8**), the obtained deep blue solution of $\{cryptand(Na^+)\}[Sn^{II}Pc(3-)]^{\bullet-}$ was filtered into a flask containing $Fe_3(CO)_{12}$ (21 mg, 0.042 mmol), $\{CpMo(CO)_3\}_2$ (12 mg, 0.024 mmol), $\{Cp^*RhCl_2\}_2$ (14 mg, 0.022 mmol), and $Ph_5CpRu(CO)_2Cl$ (28 mg, 0.044 mmol), respectively. Each solution was stirred for 1 d at 80 °C, and their deep blue color remained unchanged. Each solution was then cooled to RT and filtered into a tube for diffusion. Black plates for **7**, and blocks for **5**, **6**, and **8**, all with a characteristic copper luster, were obtained in 61%, 58%, 52%, and 69% yields, respectively.

Computational details

DFT calculations based on the M11 functional[21] were performed using the cc-pVDZ (C, H, N, and O),[22] cc-pVTZ (Fe),[23] and cc-pVTZ-PP (Ru and Sn)[24] basis sets. For the geometries of the $[CpFe(CO)_2(SnPc)]^-$ anion, $Ph_5CpRu(CO)_2(SnPc)$, and the $[Ph_5CpRu(CO)_2(SnPc)]_2$ dimer, only the coordinates of the hydrogen atoms were optimized from the X-ray structures with "Opt = Tight." For the ^1A state of $[CpFe(CO)_2(SnPc)]^-$ anion, full geometry optimization was also performed at the same level of theory. In the present DFT calculations, "Int = SuperFineGrid" was specified, and the stabilities of the wave functions were confirmed by specifying the "Stable=Opt" keyword. The subsequent natural bond orbital (NBO) analysis was performed using the NBO program.[25] All of the computations were performed with the Gaussian 09 program package.[19]

Supporting information: Equipment used, crystallographic data, and IR spectra of **1**−**8**; structural views for **1**, **2**, and **3**; details of DFT calculations for **4** and **8**; and data for magnetic measurement

data for **1** and **3**−**8** using SQUID and EPR are available free of charge via the Internet at http://pubs.acs.org.

Author information

Corresponding author

*E-mail for D.V.K.: konarev@icp.ac.ru.

Notes

The authors declare no competing financial interest.

Acknowledgments

The work was supported by RFBR grant № 13-03-00769 and JSPS KAKENHI Grant Numbers 15K17901, 23225005, and 26288035. Y.N. receives a research grant from the JGC-S Scholarship Foundation. Theoretical calculations were performed at the Research Center for Computational Science, Okazaki, Japan.

References

1. (a) Nyokong, T. *Coord. Chem. Rev*., **2007**, *251*, 1707−1722; (a) Placencia, D.; Wang, W.; Gantz, J.; Jenkins, J. L.; Armstrong, N. R. *J. Phys. Chem. C*, **2011**, *115*, 18873–18884; (c) Inabe T., Tajima, H. *Chem. Rev*. **2004**, *104*, 5503−5534; (d) Rittenberg, D. K.; Baars-Hibbe, L.; Böhm, A. B.; Miller, J. S. *J. Mater. Chem*. **2000**, *10*, 241–244; (e) Konarev, D.V.; Zorina, L.V.; Khasanov, S.S.; Hakimova, E.U.; Lyubovskaya, R.N. *New J. Chem*., **2012**, *36*, 48-51.
2. Contakes, S. M.; Beatty, S. T.; Dailey, K. K.; Rauchfuss, T. B.; Fenske, D. *Organomet.* **2000,** *19,* 4767−4774.
3. (a) Dailey, K. K.; Rauchfuss, T. B., Yap, G.P.A.; Rheingold, A.L. *Angew. Chem., Intl. Ed. Engl.* **1996**, *35*, 1833−1835; (b) Dailey, K. K.; Rauchfuss, T. B. *Polyhedron* **1997**, *16*, 3129−3136.
4. (a) Onaka, S.; Kondo, Y.; Yamashita, M.; Tatematsu, Y.; Kato, Y.; Goto, M.; Ito, T. *Inorg. Chem.* **1985**, *24*, 1070−1076; (b) Zhong, X.; Feng, Y.; Ong, S.-L.; Hu, J.; Ng, W.-J.; Wang,

Z. *Chem. Commun*. **2003**, 1882−1883; (c) Richard, P.; Zrineh, A.; Guilard, R.; Habbou, A.; Leconte, C. *Acta Cryst. Sec. C* **1989**, *45*, 1224–1226.

5. (a) Frampton, S.C., Silver J. *Inorg. Chem. Acta*, **1986**, *112*, 203–204; (b) Kato, S.; Noda, I.; Mizuta, M.; Itoh Y., *Angew. Chem. Int. Ed. Engl.* **1979**, *18*, 82–83.
6. (a) Goldner, M.; Huckstadt, H.; Murray, K. S.; Moubaraki, B.; Homborg, H. *Z. Anorg. Allg. Chem.* **1998**, *624*, 288–294; (b) Barbe, J. -M.; Morata, G.; Espinosa, E.; Guilard, R. *J. Porph. Phth.* **2003**, *7*, 120–124; (c) Yang, C. -H.; Dzugan, S. J.; Goedken, V. L. *Chem. Commun.* **1986**, *24*, 1313–1315; (d) Guilard, R.; Kadish, K. M. *Comments Inorg. Chem.* **1988**, *7*, 287–305.
7. Konarev, D. V.; Troyanov, S. I.; Kuzmin, A.V.; Nakano, Y.; Khasanov, S. S.; Otsuka, A.; Yamochi, H.; Saito, G.; Lyubovskaya, R. N. *Organometallics,* **2015**, *34*, 879-889.
8. (a) Konarev, D. V.; Khasanov, S. S.; Ishikawa, M.; Otsuka, A.; Yamochi, H.; Saito, G.; Lyubovskaya, R.N. *Inorg. Chem*., 2013, **52**, 3851-3859; (b) Konarev, D. V.; Kuzmin, A. V.; Khasanov, S. S.; Lyubovskaya, R. N. *Dalton Trans*., **2013**, *42*, 9870 – 9876; (c) Konarev, D. V.; Kuzmin, A. V.; Ishikawa, M.; Nakano, Y.; Faraonov, M. A.; Khasanov, S. S.; Otsuka, A.; Yamochi, H.; Saito, G.; Lyubovskaya, R. N. *Eur. J. Inorg. Chem.,* **2014**, 3863-3870; (d) Konarev, D.V.; Kuzmin, A. V.; Khasanov, S. S.; Otsuka, A.; Yamochi, H.; Saito, G.; Lyubovskaya, R. N. *Dalton Trans*., **2014**, *43*, 13061-13069; (e) Konarev, D. V.; Kuzmin, A. V.; Faraonov, M. A.; Ishikawa, M.; Nakano, Y.; Khasanov, S. S.; Otsuka, A.; Yamochi, H.; Saito, G.; Lyubovskaya R. N. *Chem. Eur. J.,* **2015**, *21*, 1014-1028; (f) Konarev, D. V. ; Troyanov, S. I. ; Ishikawa, M. ; Otsuka, A.; Yamochi, H. ; Saito, G. ; Lyubovskaya, R. N. *J. Porph. Phth*., **2014**, *18*, 1157-1163; (g) Konarev, D.V. ; Zorina, L.V. ; Ishikawa, M. ; Khasanov, S.S.; Otsuka, A. ; Yamochi, H. ; Saito, G. ; Lyubovskaya, R. N. *Cryst. Groth Des*., **2013**, *13*, 4930−4939; (h) Konarev, D. V.; Khasanov, S. S.; Lyubovskaya, R. N. *Coord. Chem. Rev*., **2014**,

262, 16–36.

9. (a) Nyokong, T. *Polyhedron*, **1994**, *13*, 2067-2071; (b) Lever, A. B. P.; Milaeva, E. R.; Speier, G. In Phthalocyanines: Properties and Applications. Eds. Leznoff, C. C.; Lever, A. B. P.; **1993**, Vol. 3, VCH Publishing, Weinheim. P. 1-70.
10. Lever, A.B.P. *Adv. Inorg. Chem. Radiochem*., **1965**, *7*, 27-114.
11. (a) Alonso, M.; Alvarez, M. A.; García, M. E.; Ruiz, M. A.; Hamidov, H.; Jeffery, J. C. *J. Am. Chem. Soc*., **2005**, *127*, 15012–15013; (b) Boyle, T. J.; Takusagawa, F.; J. A. Heppert *Acta Crystallogr., Sect. C: Cryst. Struct. Commun.,* **1990**, *46*, 892-893; (c) Drew, M. G. B.; Félix, V.; Romão, C. C.; Royo B. *J. Chem. Soc., Dalton Trans.,* **2002**, 584-590.
12. (a) Yasuda, R.; Iwasa, K.; Niikura, F.; Seino, H.; Mizobe, Y. *Dalton Trans*., **2014**, *43*, 9344-9355; (b) Schaper, L.-A.; Wei, X.; Altmann, P. J.; Öfele, K.; Pöthig, A.; Drees, M.; Mink, J.; Herdtweck, E.; Bechlars, B.; Herrmann, W. A.; Kühn, F. E. *Inorg. Chem*. **2013**, *52*, 7031–7044; (c) Davidson, J. L.; Wilson, W. F.; Manojlović-Muir, L.; Muir K. W. *J. Organomet. Chem*., **1983**, *254*, C6-C10.
13. Yang, F.; Yu, P.; Zhao, J.; Shi , J.; Wang, J. *Phys. Chem. Chem. Phys*., **2015**,*17*, 14542-14550.
14. Kubiak, R.; Janczak, J. *J. Alloys Compd*. **1992**, *189*, 107–111.
15. Konarev, D.V.; Zorina, L.V.; Khasanov, S. S.; Litvinov, A. L.; Otsuka, A.; Yamochi, H.; Saito, G.; Lyubovskaya, R.N. *Dalton Trans.,* **2013**, *42*, 6810-6816.
16. (a) van der Eide, E. F.; Hou, G.-L.; Deng, S. H. M.; Wen, H.; Yang, P.; Bullock, R. M.; Wang, X.-B. *Organometallics*, **2013**, *32*, 2084−2091; (b) Gasanov, R. G.; Lobach, A. S.; Sokolov, V. I.; Demenjev, A. P.; Maslakov K. I.; Obraztsova, E. D. *J. Nanosci. Nanotechno.,* **2007**, *7*, 1-5.
17. (a) Thompson, D. M.; Jones, M.; Baird, M. C. *Eur. J. Inorg. Chem.* **2003**, 175-180; (b)

Konarev, D. V.; Kuzmin, A. V.; Troyanov, S. I.; Nakano, Y.; Khasanov, S. S.; Otsuka, A.; Yamochi, H.; Saito, G.; Lyubovskaya, R. N. *Dalton Trans*., **2015**, *44*, 9672-9681.

18. Smart, J. S. "Magnetism III", eds by Rado, G.T.; Suhl, H. Academic Press, NY, **1963**, p. 63.

19. Gaussian 09, Revision D.01, Frisch, M. J.; Trucks, G. W.; Schlegel, H. B.; Scuseria, G. E.; Robb, M. A.; Cheeseman, J. R.; Scalmani, G.; Barone, V.; Mennucci, B.; Petersson, G. A.; Nakatsuji, H.; Caricato, M.; Li, X.; Hratchian, H. P.; Izmaylov, A. F.; Bloino, J.; Zheng, G.; Sonnenberg, J. L.; Hada, M.; Ehara, M.; Toyota, K.; Fukuda, R.; Hasegawa, J.; Ishida, M.; Nakajima, T.; Honda, Y.; Kitao, O.; Nakai, H.; Vreven, T.; Montgomery, Jr. J. A.; Peralta, J. E.; Ogliaro, F.; Bearpark, M.; Heyd, J.; Brothers, J. E.; Kudin, K. N.; Staroverov, V. N.; Keith, T.; Kobayashi, R.; Normand, J.; Raghavachari, K.; Rendell, A.; Burant, J. C.; Iyengar, S. S.; Tomasi, J.; Cossi, M.; Rega, N.; Millam, J. M.; Klene, M.; Knox, J. E.; Cross, J. B.; Bakken, V.; Adamo, C.; Jaramillo, J.; Gomperts, R.; Stratmann, R.; Yazyev, E. O.; Austin, A. J.; Cammi, R.; Pomelli, C.; Ochterski, J. W.; Martin, R. L.; Morokuma, K.; Zakrzewski, V. G.; Voth, G. A.; Salvador, P.; Dannenberg, J. J.; Dapprich, S.; Daniels, A. D.; Farkas, O.; Foresman, J. B.; Ortiz, J. V.; Cioslowski, J.; Fox, D. J. Gaussian, Inc., Wallingford CT, 2013.

20. Konarev, D.V.; Khasanov, S.S.; Yudanova, E. I.; Lyubovskaya, R.N. *Eur. J. Inorg. Chem.,* **2011**, 816-820.

21. Peverati, R.; Truhlar, D. G. *J. Phys. Chem. Lett.* **2011**, *2*, 2810-2817.

22. Dunning Jr., T. H. *J. Chem. Phys.* **1989**, *90*, 1007-1023.

23. Balabanov, N. B.; Peterson, K. A. *J. Chem. Phys.* **2005**, *123*, 064107/1-15.

24. a) Peterson, K. A.; Figgen, D.; Dolg, M.; Stoll, H. *J. Chem. Phys.* **2007**, *126*, 124101/1-12; b) Peterson, K. A. *J. Chem. Phys.* **2003**, *119*, 11099-11112; c) Feller, D. *J. Comp. Chem.* **1996**, *17*, 1571-1586; d) Schuchardt, K. L.; Didier, B. T.; Elsethagen, T.; Sun, L.; Gurumoorthi, V.;

Chase, J.; Li, J.; Windus, T. L. *J. Chem. Inf. Model.* **2007**, *47*, 1045-1052.

25. NBO Version 3.1, Glendening, E. D.; Reed, A. E.; Carpenter, J. E.; Weinhold, F.

SYNOPSIS

The ability of Sn atoms to form stable Sn−M bonds with transition metals was used to prepare transition metal (M = Mo, Fe, Rh, and Ru) complexes with tin(II) phthalocyanine in neutral, radical anionic, and dianionic states. The crystal structures and optical and magnetic properties of the complexes were investigated. It was found that $[Sn^{II}Pc(3-)]^{\bullet-}$ radical anions are potential anionic paramagnetic ligands for transition metals that may enable the preparation of magnetic assemblies.

For Table of Contents Only

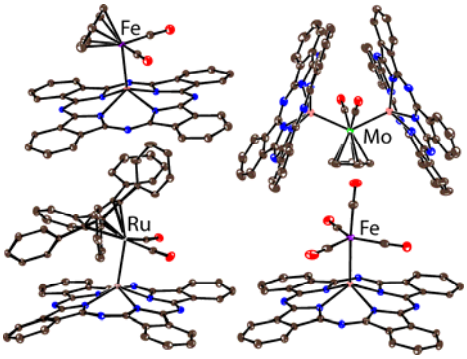

Coordination complexes of transition metals (M = Mo, Fe, Rh and Ru) with tin(II) phthalocyanine in neutral, radical anion and dianionic states

Dmitri V. Konarev,*† Alexey V. Kuzmin,‡ Yoshiaki Nakano,§ Maxim A. Faraonov,† Salavat S. Khasanov,‡ Akihiro Otsuka,§ Hideki Yamochi,§ Gunzi Saito,||, ¶ and Rimma N. Lyubovskaya†

†Institute of Problems of Chemical Physics RAS, Chernogolovka, Moscow region, 142432 Russia;

‡Institute of Solid State Physics RAS, Chernogolovka, Moscow region, 142432 Russia;

§Research Center for Low Temperature and Materials Sciences, Kyoto University, Sakyo-ku, Kyoto 606-8501, Japan;

||Faculty of Agriculture, Meijo University, 1-501 Shiogamaguchi, Tempaku-ku, Nagoya 468-8502, Japan.

¶Toyota Physical and Chemical Research Institute, 41-1, Yokomichi, Nagakute, Aichi 480-1192, Japan

SUPPORTING INFORMATION

General

UV−visible−NIR spectra were obtained using KBr pellets on a Perkin Elmer Lambda 1050 spectrometer in the 250 nm to 2500 nm range. FT−IR spectra were obtained using KBr pellets with a Perkin−Elmer Spectrum 400 spectrometer (400−7800 cm^{-1}). EPR spectra were recorded for sealed polycrystalline samples of **1**−**8** in the temperature range from 4 K to 295 K using a JEOL JES-TE 200 X-band ESR spectrometer equipped with a JEOL ES-CT470 cryostat. A Quantum Design MPMS-XL SQUID magnetometer was used to measure the static magnetic susceptibilities of **3**−**8** at a magnetic field of 100 mT under cooling and heating conditions in the range from 300 K to 1.9 K. The sample holder contribution and core temperature independent diamagnetic susceptibility (χ_d) were subtracted from the experimental values. The χ_d values were estimated by extrapolating the data in the high-temperature range (from 20−70 K up to 300 K) using the following expression: $\chi_M = C/(T - \Theta) + \chi_d$, where C is the Curie constant and Θ is the Weiss temperature. Effective magnetic moments (μ_{eff}) were calculated using the formula $\mu_{eff} = (8 \cdot \chi_M \cdot T)^{1/2}$.

X-ray crystal structure determinations

X-ray diffraction data for **1**, **3**−**8** are listed in Tables S1 and S2. X-ray diffraction data for **1** were collected on a Bruker Smart Apex II CCD diffractometer with graphite monochromated MoK_α radiation using a Japan Thermal Engineering Co. cooling system DX-CS190LD. Raw data reduction to F^2 was performed using Bruker SAINT.[1] X-ray diffraction data for **3**−**8** were collected on an Oxford diffraction "Gemini-R" CCD diffractometer with graphite monochromated MoK_α radiation using an Oxford Instrument Cryojet system. Raw data reduction to F^2 was performed using CrysAlisPro, Oxford Diffraction Ltd. The structures were solved using a direct method and refined using the full-matrix least-squares method against F^2 using SHELX-2013.[2] Non-hydrogen atoms

were anisotropically refined. The positions of hydrogen atoms were included in the refinement in a riding model.

Disorder

Complex **1** contains both Br^- anions and carbonyl ligands disordered between two positions. The occupancy of both positions is approximately 0.5, which provides a composition for **1** of $\{Cp^*MoBr(CO)_2[Sn^{II}Pc(2-)]\}\cdot 0.5C_6H_4Cl_2$. We used the following restraints: 8 DFIX to fix the length of bonds in the disordered $Cp^*MoBr(CO)_2$ groups; 4 DELU, 48 SIMU, and 48 ISOR to correct thermal ellipsoids in the same groups.

Structure **3** contains two crystallographically independent $[Sn^{II}Pc(3-)]^{\bullet-}$ radical anions, cryptand(Na^+) cations, and solvent $C_6H_4Cl_2$ molecules. Among them, only one $C_6H_4Cl_2$ molecule is disordered between two orientations with 0.864(8)/0.136(8) occupancies. We used the following restraints: 54 SAME to fix the geometry of disordered solvent $C_6H_4Cl_2$ molecule; 36 DELU, 24 SIMU, and 48 ISOR to correct thermal ellipsoids of atoms in this molecule. Refinement of the crystal structure was made using all experimental data excepting 16 hkl reflections ($F(obs)^2 - F(calc)^2$)/esd > 6.0, which were rejected using OMIT instructions.

The structure of **4** has one ordered $\{CpFe(CO)_2[Sn^{II}Pc(4-)]\}^-$ anion, whereas the cryptand(Na^+) cation is disordered between two orientations with 0.707(4)/0.293(4) occupancies. There are also three positions for the solvent $C_6H_4Cl_2$ molecules with half occupancy. All of them are disordered between two orientations with 0.377(3)/0.123(3), 0.344(3)/0.156(3) and 0.275(3)/0.225(3) occupancies. We used the following restraints: 270 SAME to fix geometry of disordered solvent $C_6H_4Cl_2$ molecules; 387 DELU was used for all atoms in the unit cell; 132 SIMU, and 348 ISOR to correct thermal ellipsoids of disordered cryptand(Na^+) cation and solvent $C_6H_4Cl_2$ molecules. Refinement of the crystal structure was made using all experimental data excepting 12 hkl reflections ($F(obs)^2 - F(calc)^2$)/esd > 5.0, which were rejected using OMIT instructions.

One of two independent cryptand(Na^+) cations with 0.5 occupation is strongly disordered in **5** between three orientations with 0.267(3)/0.156(2)/0.077(2) occupancies, whereas the solvent $C_6H_4Cl_2$ molecule with 0.5 occupancy is disordered between two orientations (0.39/0.11). We used the following restraints: 369 SAME to fix geometry of strongly disordered cryptand(Na^+) cation; 966 SIMU, and 468 ISOR to correct thermal ellipsoids in disordered cryptand(Na^+) cation.

The cryptand(Na^+) cation is disordered in **6** with 0.633(4)/0.367(4) occupancies. There are four positions for the solvent $C_6H_4Cl_2$ molecules in **6**. In two positions with full occupancy, they are disordered between two orientations with 0.715(6)/0.285(5) and 0.704(5)/0.296(5) occupancies. Ordered $C_6H_4Cl_2$ molecules occupy two positions with full and half occupancies. We used the following restraints: 381 SAME to fix geometry of disordered cryptand(Na^+) cation and solvent $C_6H_4Cl_2$ molecules. 468 SIMU, and 180 ISOR to correct thermal ellipsoids of the C, N, O и Cl atoms for the disordered cryptand(Na^+) cation and solvent $C_6H_4Cl_2$ molecules. 10 FLAT were used for additional correction of the geometry of the disordered $C_6H_4Cl_2$ molecules.

We used the following restraints for the refinement of crystal structure of **7**: 111 DELU, 144 and ISOR to correct thermal ellipsoids of the C, N, O atoms of cryptand(Na^+) cation.

All components are ordered in the crystal structure of **8**. No restraints are used for the refinement of this crystal structure.

References.

1. Bruker Analytical X-ray Systems, Madison, Wisconsin, U.S.A, **1999.**
2. Sheldrick, G. M. *Acta Cryst. Sect. C.* 2015, **71**, 3-8

Table S1. Crystallographic data and some details of data collection and refinement for **1-4**.

Compound	**1**	**3**	**4**
Empirical formula	$C_{47}H_{33}BrCl\ MoN_8O_2\ Sn$	$C_{56}H_{56}Cl_2N_{10}NaO_6Sn$	$C_{66}H_{63}Cl_3FeN_{10}NaO_8Sn$
M_r [g·mol^{-1}]	1071.80	1177.68	1428.14
Crystal color and shape,	Black prism	Black parallelepiped	Black prism
Crystal system	Triclinic	Orthorhombic	Monoclinic
Space group	$P\ \bar{1}$	$P\ 2_12_12_1$	$P\ 2_1/n$
a, Å	12.5315(2)	13.4963(2)	11.3884(3)
b, Å	13.2913(2)	22.4928(2)	22.9569(7)
c, Å	13.5195(2)	34.7416(5)	23.6336(7)
α, °	91.901(1)	90	90
β, °	92.247(1)	90	90.574(2)
γ, °	112.733(1)	90	90
V, Å^3	2072.42(6)	10546.5(2)	6178.5(3)
Z	2	8	4
ρ_{calc} [g/cm^3]	1.718	1.483	1.535
μ [mm^{-1}]	1.985	0.656	0.842
F(000)	1062	4840	2924
T [K]	150(2)	150(2)	150(2)
2Θ, °	58.220	56.604	56.58
Reflns measured	20043	114428	55582
Unique reflns	9997	25297	14627
Params/Restraints	607/108	1418/162	1046/1137
Reflns [F_o>2σ(F_o)]	9055	19692	10741
R_1 [F_o>2σ(F_o)]/wR_2 all)[a]	0.0343/0.1006	0.0592/0.1502	0.0472/0.1172
G.O.F	1.072	1.043	1.021
CCDC number	1409661	1413374	1413375

(a) $w = 1/[\sigma^2(F_o^2) + (aP)^2 + bP]$, $P = [Max(F_o^2,0) + 2F_c^2]/3$

Table S2. Crystallographic data and some details of data collection and refinement for **5-8**.

Compound	**5**	**6**	**7**	**8**
Empirical formula	$C_{168}H_{160}Cl_2Fe_3N_{30}Na_3O_{30}Sn_3$	$C_{110}H_{87}Cl_7MoN_{18}NaO_8Sn2$	$C_{66}H_{71}Cl_4N_{10}NaO_6RhSn$	$C_{69}H_{41}N_8O_2RuSn$
M_r [g·mol^{-1}]	3742.81	2393.43	1486.71	1233.86
Crystal color and shape,	Black block	Black block	Black plate	Black block
Crystal system	Monoclinic	Triclinic	Monoclinic	Triclinic
Space group	$P\,2_1/m$	$P\,\bar{1}$	$P\,2_1$	$P\,\bar{1}$
a, Å	13.3558(3)	17.0023(4)	13.0896(1)	11.9653(4)
b, Å	37.2399(6)	17.4314(5)	26.0217(3)	12.4086(5)
c, Å	16.3799(3)	17.7859(3)	18.9023(2)	19.4571(6)
α, °	90	85.695(2)	90	75.005(3)
β, °	98.649(2)	88.189(2)	95.741(1)	72.626(3)
γ, °	90	77.512(2)	90	73.457(3)
V, Å^3	8054.2(3)	5131.4(2)	6406.09(11)	2594.84(17)
Z	2	2	4	2
ρ_{calc} [g/cm^3]	1.543	1.549	1.542	1.579
μ [mm^{-1}]	0.847	0.858	0.882	0.832
F(000)	3826	2418	3036	1242
T [K]	150(2)	150(2)	180(2)	150(2)
2Θ, °	58.062	58.096	58.742	58.206
Reflns measured	65899	44402	57412	22242
Unique reflns	19416	23517	28726	11953
Params/Restraints	1526/1804	1589/1039	1579/256	730/0
Reflns [$F_o>2\sigma(F_o)$]	14365	14971	23680	10019
R_1 [$F_o>2\sigma(F_o)$]/wR_2 all)[a]	0.0587/0.1322	0.0623/0.1779	0.0477/0.0964	0.0312/0.0775
G.O.F	1.000	1.028	1.031	1.057
CCDC number	1409659	1409663	1409651	1409662

(a) $w = 1/[\sigma^2(F_o^2) + (aP)^2 + bP]$, $P = [Max(F_o^2,0) + 2F_c^2]/3$

Table S3. IR spectra of starting compounds, salt **3** and coordination complex **1**.

Components	$Sn^{II}Pc(2-)$	Cryptand [2,2,2]	{cryptand(Na^+)} $[Sn^{II}Pc(3-)]^{\bullet-}$ $\cdot C_6H_4Cl_2$ (**3**)	$\{Cp^*Mo(CO)_2\}_2$	$\{Cp^*Mo(Br)(CO)_2$ $[Sn^{II}Pc(2-)]\}$ $\cdot 0.5C_6H_4Cl_2$ (**1**)	$\{CpFe(CO)_2\}_2$
Tin phthalocyanine	435w 498w 627w 725m 745m 768m 819w 872w 887m 948w 1059s 1072s 1114s 1156w 1283m 1329s 1407w 1454w 1486s 3049w		437w 497w 629w 717s 747s* 766m 818w - 886w* 942w* - 1072s* 1116s* - 1286m* 1332m 1418w 1457s* 1501w* 3053w		436w 503w 630w 725s 749m 774m 824w 874w 891m 954w - 1076s 1117s 1161w 1286m 1332s 1418w* 1459w* - 3057w	
$Cryptand(Na)^+$		476w 528w 581w 735m 922m 948w 982m 1038w 1071m 1100s 1127s 1213w 1295m 1329m 1360s 1446m 1462m 1490w - 2790w 2877w 2943w	467w 536w 564w 733m 926w 942w* 986w* 1043m 1072s 1103s 1116s* - 1286m* 1332m* 1356m 1440s 1457s* 1501s 1537m 2812w 2866w 2960w			
Transition metal fragment				495w 531s 1027m 1384s 1416w 1450w 1478w CO 1825s 1870s CH 2918w 2970w	503w* - 1021w 1382m* 1418w* 1459w* 1478w* CO 1852s 1937s CH 2918w 2959w	542w 565w 595w 648m 830w 1016w - - CO 1756s 1771s 1936s 1956s CH 3113w
Solvent			658w 747s* 1032w 1457s*		- - 1031w 1459w*	

* - bands are coincided; w – weak intensity, m –middle intensity, s – strong intensity

Table S4. IR spectra of starting compounds and coordination complexes **3-6**.

Components	{$CpFe(CO)_2$ [$Sn^{II}Pc(2-)$]} $\cdot 2C_6H_4Cl_2$ (**2**)	{cryptand(Na^+)} {$CpFe(CO)_2$ [$Sn^{II}Pc(4-)$]}$^-$ $\cdot C_6H_4Cl_2$ (**4**)	{$CpMo(CO)_3$}$_2$	{cryptand(Na^+)} {$CpMo(CO)_2$ [$Sn^{II}Pc(2-)Sn^{II}Pc(3-)^{\bullet -}$]} $\cdot 3.5C_6H_4Cl_2$ (**6**)	$Fe_3(CO)_{12}$	{cryptand(Na^+)} {$Fe(CO)_4$ [$Sn^{II}Pc(3-)]^{\bullet -}$} $\cdot 1/3C_6H_4Cl_2$ (**5**)
Tin phthalocyanine	436w	439w		432w		437w
	502w	491w		502w*		498w
	627w	632w		-		625s
	705m	698s		710s		-
	727s	738m*		729m*		712m
	748m*	748s*		747m*		747m*
	-	-		761m		770m
	821w	820w		816w		821w
	-	877w		-		-
	891w	-		890w		891w
	949m	941w*		941w*		941w*
	1055m	1054s		1057m		1053w
	1084m	-		1080s*		1088s
	1114s	1133m*		1116s*		1117s*
	1164w	1165w		1165m		1165m
	1261w	1262w		1265w*		1263w
	1300m	1304s*		1332s*		1330m*
	1419m	1418s*		1418m*		1421w
	1465w*	1456s*		1454m*		1464m*
	1485w	-		-		-
	3056w	3047w		3054w		3051w
Cryptand(Na^+)						
		474w		484w*		-
		-		-		-
		583m		-		-
		738m*		729m*		730w
		-		-		927w
		941w*		941w*		941w*
		984w		-		-
		-		1034w*		1037w*
		-		1080s*		-
		1096s		-		1102s
		1133m*		1116s*		1117s*
		1218w		-		-
		-		1288m		1300m
		1304s		1332s*		1330m*
		1355m		1355w		1355w
		1456s*		1454m*		1436m
		-		1497w		1464m*
		-		1537w		1500w
		2809w		2817w		2816w
		2870w		2868w		2898w
		2961w		2951w		2962w
Transition metal fragment	-	-	417w	420w	592s	568w
	568w	570w	451m	446m	CO	CO
	582w	-	477w	484w*	1852s	1908s sp
	660w*	658w*	501m	502w*	1859s	1933s sp
	830w	828w	547m	558m	2029s	2012s
	-	-	587m	-		
	1609s	1553s	824s	824w		\
	1621s	1568m	1016w	-		
	CO	CO	1264w	1265w*		
	1961s	1942s	1419w	1418m*		
	2012s	1961m	1427w	-		
	C-H	2006s	CO	CO		
	3162w	C-H	1886s	1856s		
		3166w	1899s	-		
Solvent	660w*		1953s	1923m		
	748m*	658w*	3115w (C-H)			
	1032w	748s*		-		-
	1465w*	1033w		747m*		747m*
		1456s*		1034w*		1037w*
				1454m*		1464m*

* - bands are coincided; sp - split band, w – weak intensity, m –middle intensity, s – strong intensity

Table S5. IR spectra of starting compounds and coordination complexes **7** and **8**.

Components	$\{Cp^*RhCl_2\}_2$	$\{cryptand(Na^+)\}\{Cp^*RhCl_2[Sn^{II}Pc(3-)]^{\bullet-}\}\cdot C_6H_4Cl_2$ (**7**)	$Ph_5CpRu(CO)_2Cl$	$\{Ph_5CpRu(CO)_2[Sn^{II}Pc(3-)]\}$ (**8**)
Tin phthalocyanine		438w 498w 632w 714s 747s* 765m 821w - 887w* 944w* 1054w 1088m* 1113s* 1165m* 1288m* 1328m 1419m 1456s* 1497w* 3052w		439w 501w* - 728m 745m* 761m 827w 868w 890w 948w - 1079w* 1118s 1163m* 1288w 1328s 1417m 1466w* - 3057w
$Cryptand(Na)^+$		471w 536w* 583w* 731w 926w 944w* 1032w* 1088m* 1101s 1113s* 1288m* 1328m* 1355w 1437m 1456s* 1497w* C-H 2812w 2863w 2962w		
Transition metal fragment	420w 451w 587w 619w 879w 1029s 1078m 1162m 1369s 1456s C-H 2915w 2966w 2987w	421w 450w 583w* 613w 887w* 1032w* 1088m* 1165m* 1376w 1456s* C-H 2915w 2962w -	458w 494w 503w 539w 561m 573s - 700s 739s 783w 1031w 1074w 1157w 1263w 1445m 1502m CO 1990s 2042s C-H 2971w 3062w	477w 487w 501w* 537w 559m 568s 607s 704s 738m* 798w 1030w* 1079w* 1163m* - 1445m 1501m CO 1978s 2026s C-H 2962w 3057w
Solvent		658w 747s 1032w* 1456s*		- 745m* 1030w* 1466w*

* - bands are coincided, w – weak, m –middle, s – strong intensity

IR spectra of starting metal phthalocyanines and their anion-radical salts.

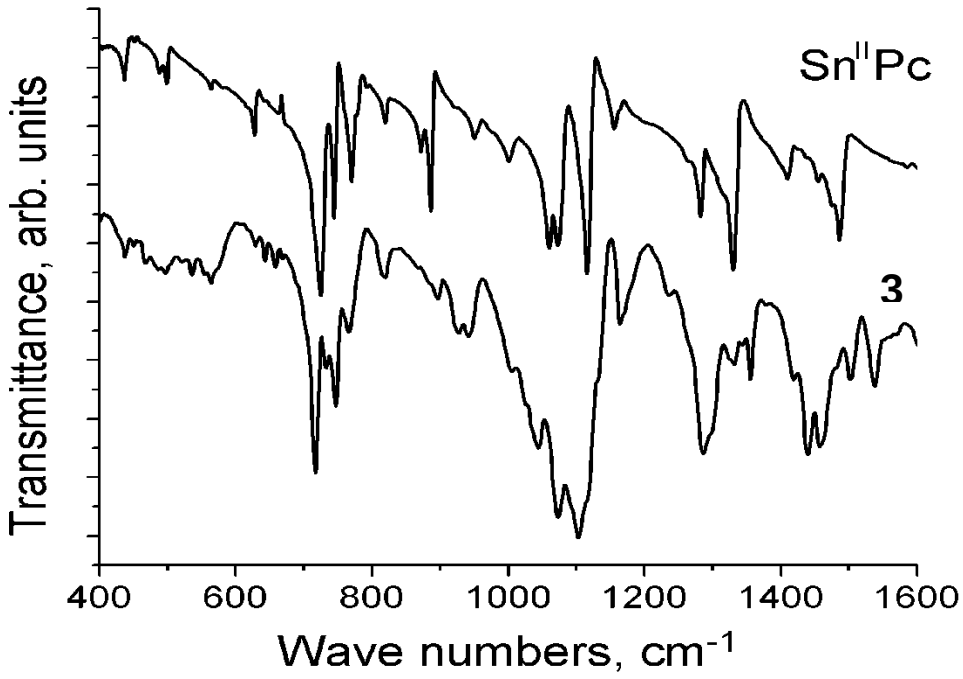

Figure S1. IR spectra of starting neutral tin(II) phthalocyanine $[Sn^{II}Pc(2-)]^0$ and salt $\{cryptand(Na^+)\}[Sn^{II}Pc(3-)]^{\bullet-}\cdot C_6H_4Cl_2$ (**3**) in KBr pellet prepared in anaerobic condition.

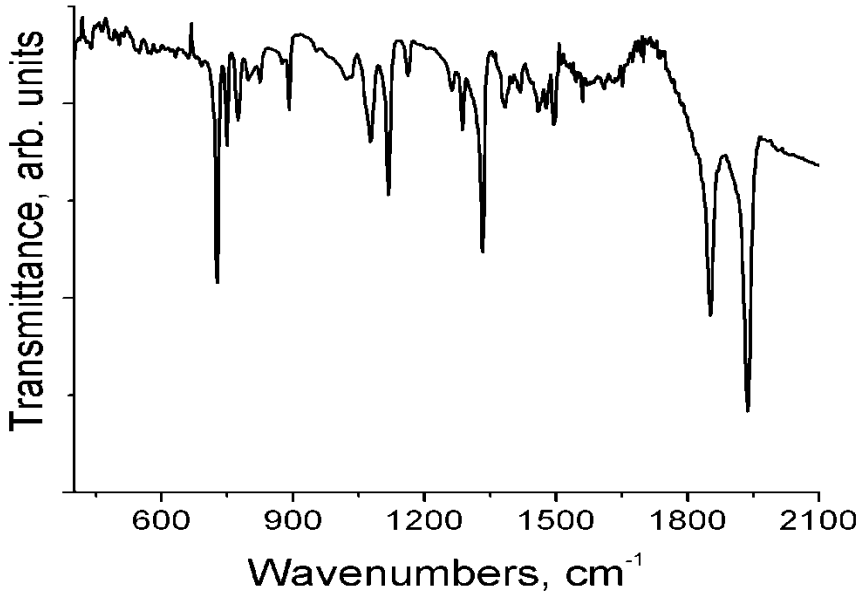

Figure S2. IR spectrum of neutral coordination complex $\{Cp^*Mo(Br)(CO)_2[Sn^{II}Pc(2-)]\}\cdot 0.5C_6H_4Cl_2$ (**1**) in KBr pellet prepared in anaerobic condition.

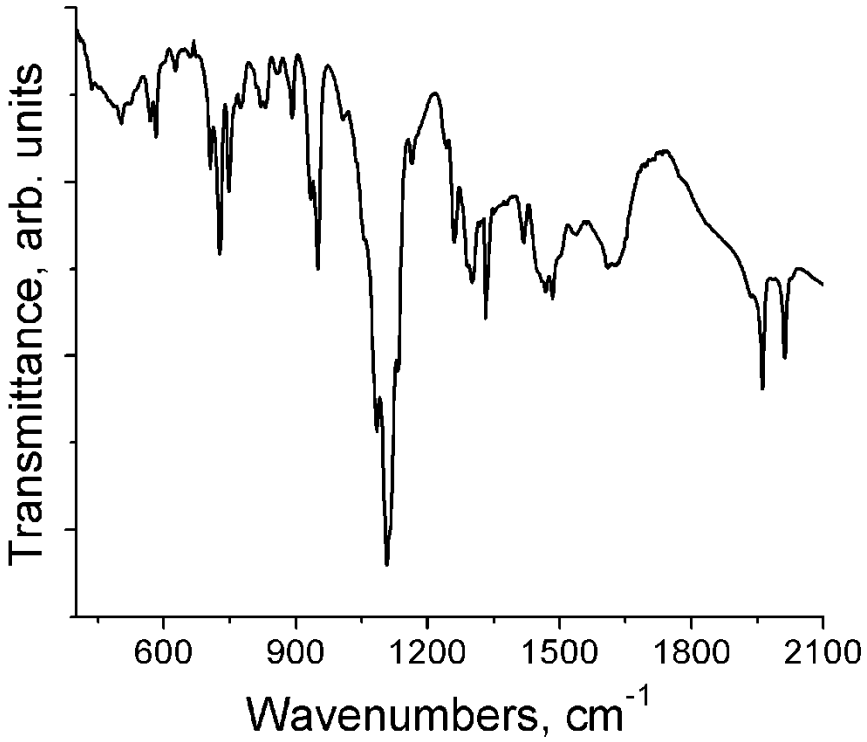

Figure S3. IR spectrum of neutral coordination complex $\{CpFe(CO)_2[Sn^{II}Pc(2-)]\}\cdot 2C_6H_4Cl_2$ (**2**) in KBr pellet prepared in anaerobic condition.

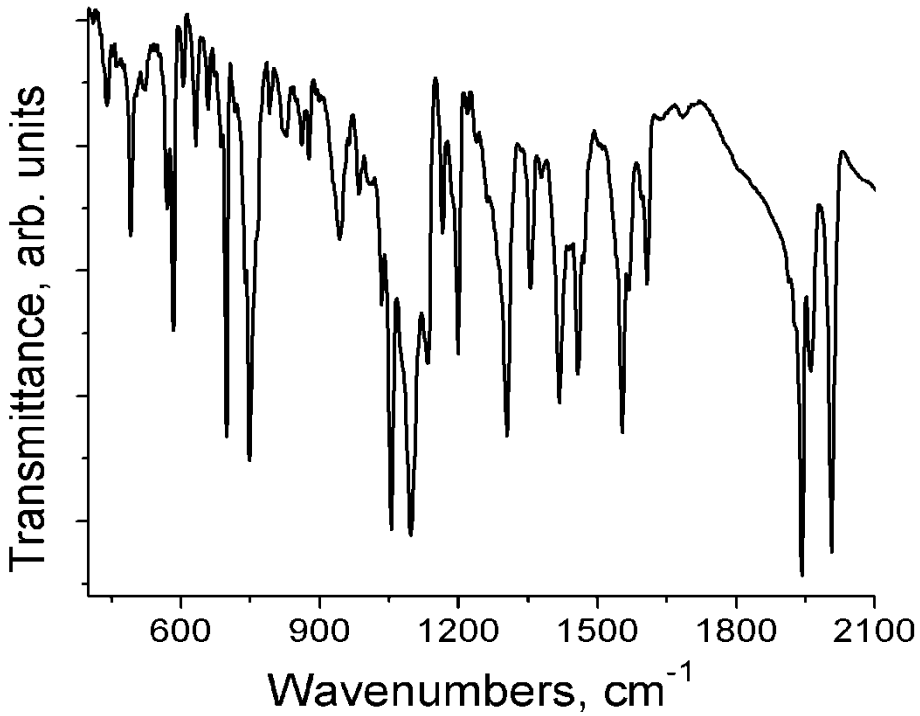

Figure S4. IR spectrum of $\{cryptand(Na^+)\}\{CpFe(CO)_2[Sn^{II}Pc(4-)]\}^-\cdot C_6H_4Cl_2$ (**4**) in KBr pellet prepared in anaerobic condition.

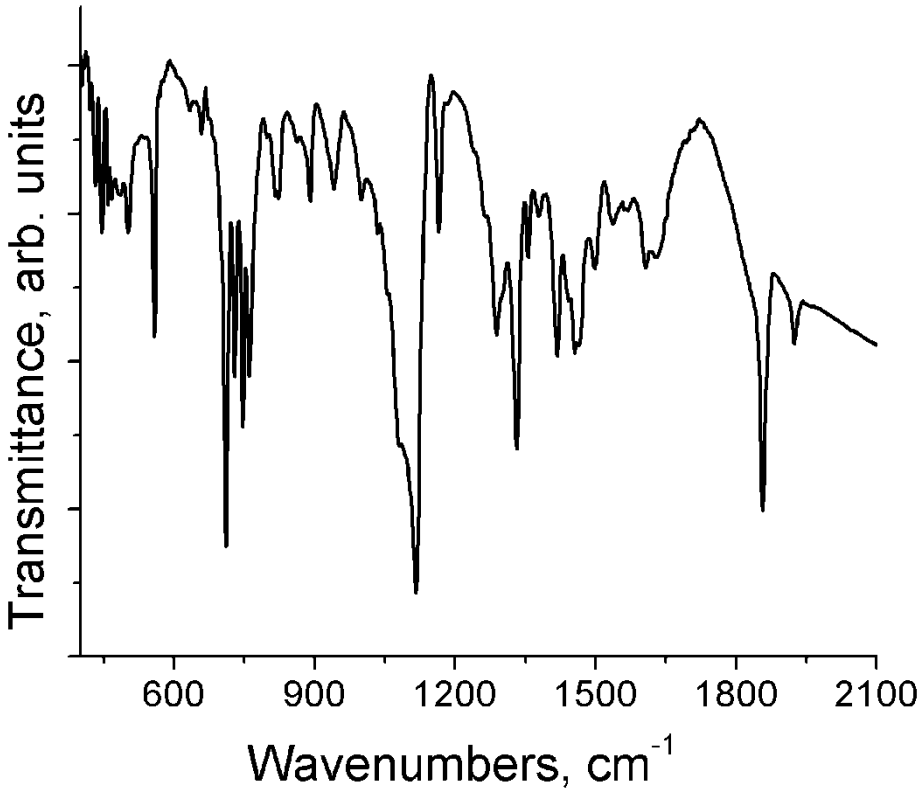

Figure S5. IR spectrum of {cryptand(Na^+)}{$CpMo(CO)_2[Sn^{II}Pc(2–)Sn^{II}Pc(3–)^{\bullet-}]$}·$3.5C_6H_4Cl_2$ (**6**) in KBr pellet prepared in anaerobic condition.

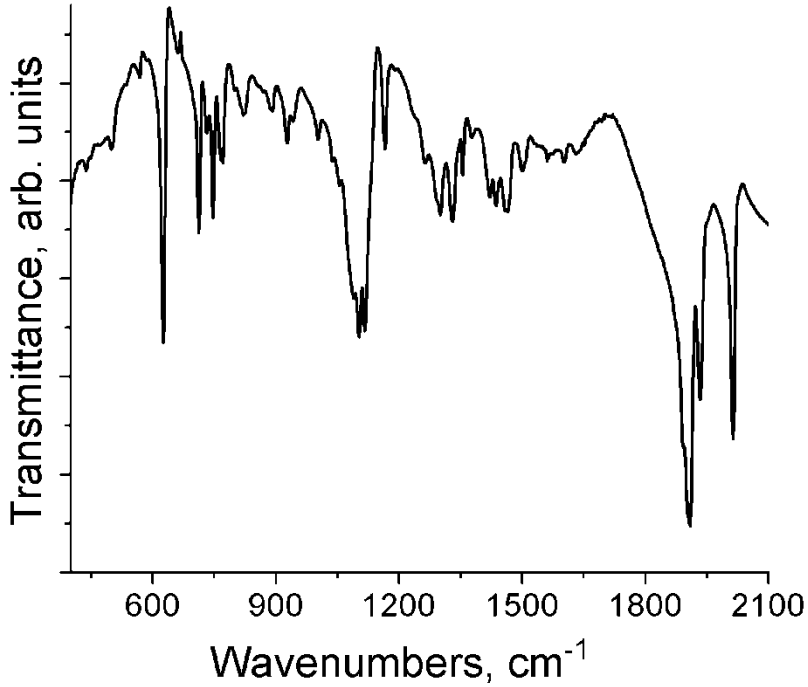

Figure S6. IR spectrum of {cryptand(Na^+)}{$Fe(CO)_4[Sn^{II}Pc(3-)]^{\bullet-}$}·$1/3C_6H_4Cl_2$ (**5**) in KBr pellet prepared in anaerobic condition.

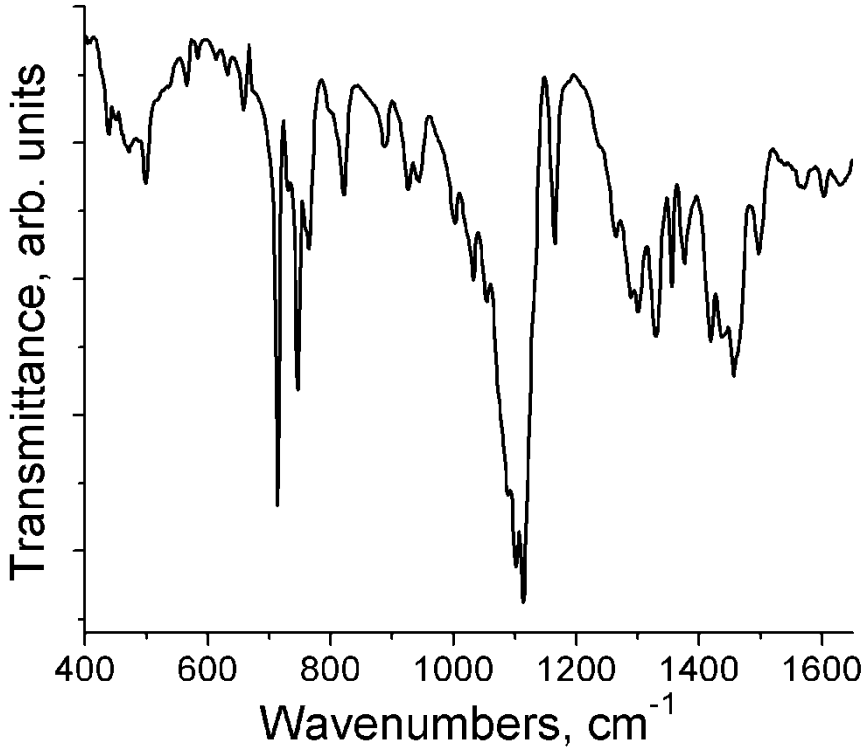

Figure S7. IR spectrum of anionic coordination complex {cryptand(Na^+)}{Cp^*RhCl_2 $[Sn^{II}Pc(3-)]^{\bullet-}$}·$C_6H_4Cl_2$ (**7**) in KBr pellet prepared in anaerobic condition.

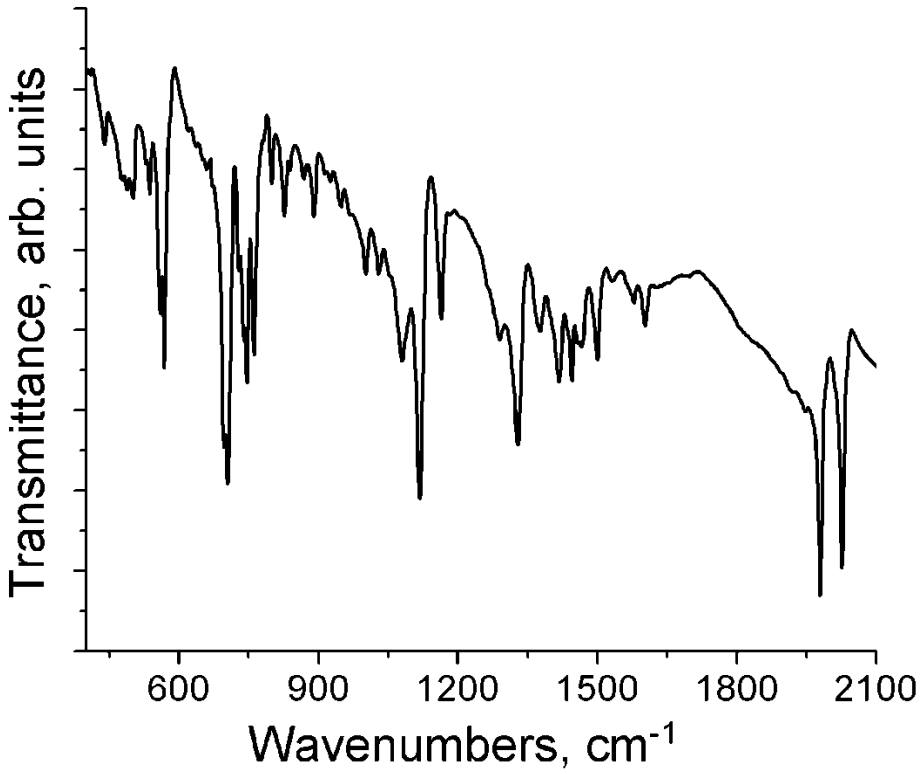

Figure S8. IR spectrum of {$Ph_5CpRu^{II}(CO)_2[Sn^{II}Pc(3-)]$} (**8**) in KBr pellet prepared in anaerobic condition.

Crystal structures of the salts.

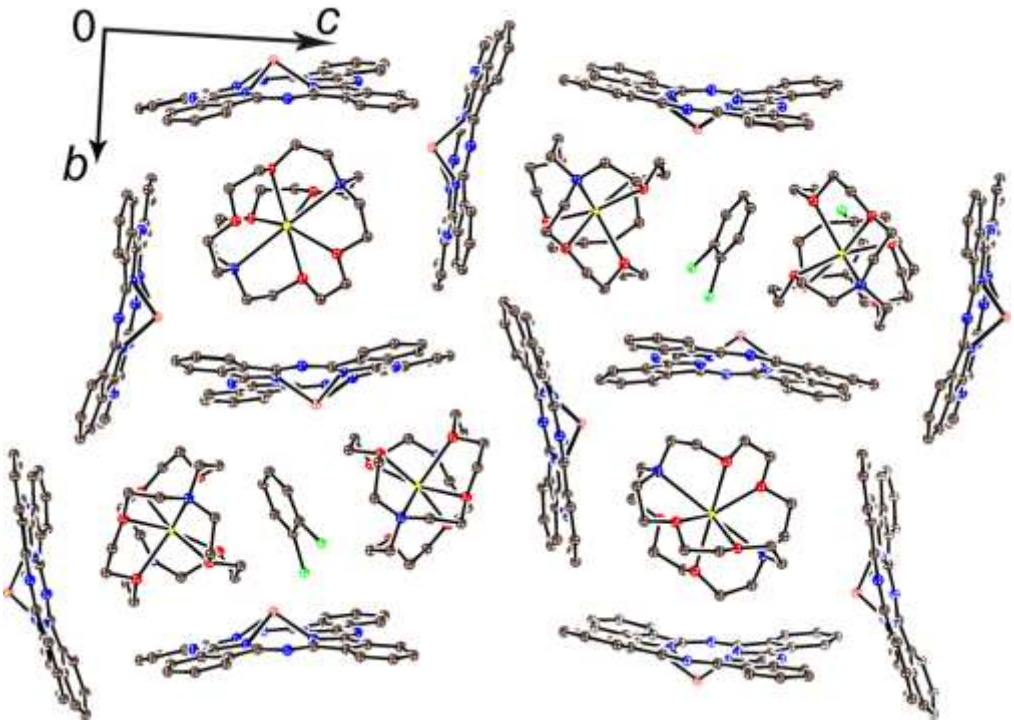

Figure S9. View along the *a*-axis on two types of channels formed by the $[Sn^{II}Pc(3–)]^{\bullet-}$ planes in $\{cryptand(Na^{+})\}[Sn^{II}Pc(3-)]^{\bullet-}\cdot C_6H_4Cl_2$ (**3**). The two type of channels occupied by the cryptand(Na^{+}) cations or by the cryptand(Na^{+}) cations and solvent $C_6H_4Cl_2$ molecules.

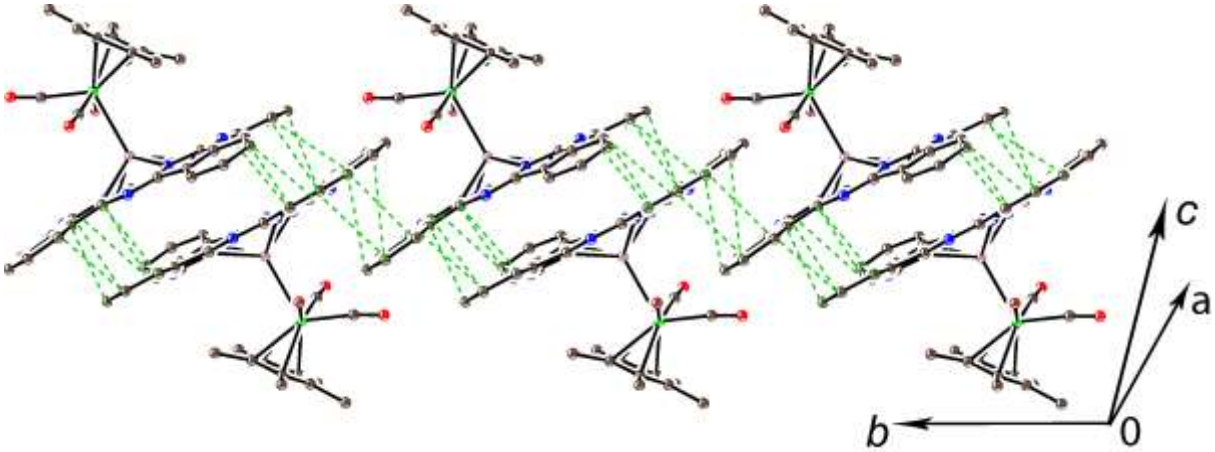

Figure S10. Crystal structure of $Cp^*Mo(Br)(CO)_2[Sn^{II}Pc(2-)]\cdot 0.5C_6H_4Cl_2$ (**1**), view on the chain from the π-stacking dimers formed by two coordination units. Van der Waals C,N···C,N contacts between Pc planes are shown by green dashed lines.

Data of magnetic measurement by SQUID and EPR .

{Cryptand(Na^+)}[$Sn^{II}Pc(3-)]^{\bullet-}\cdot C_6H_4Cl_2$ (3)

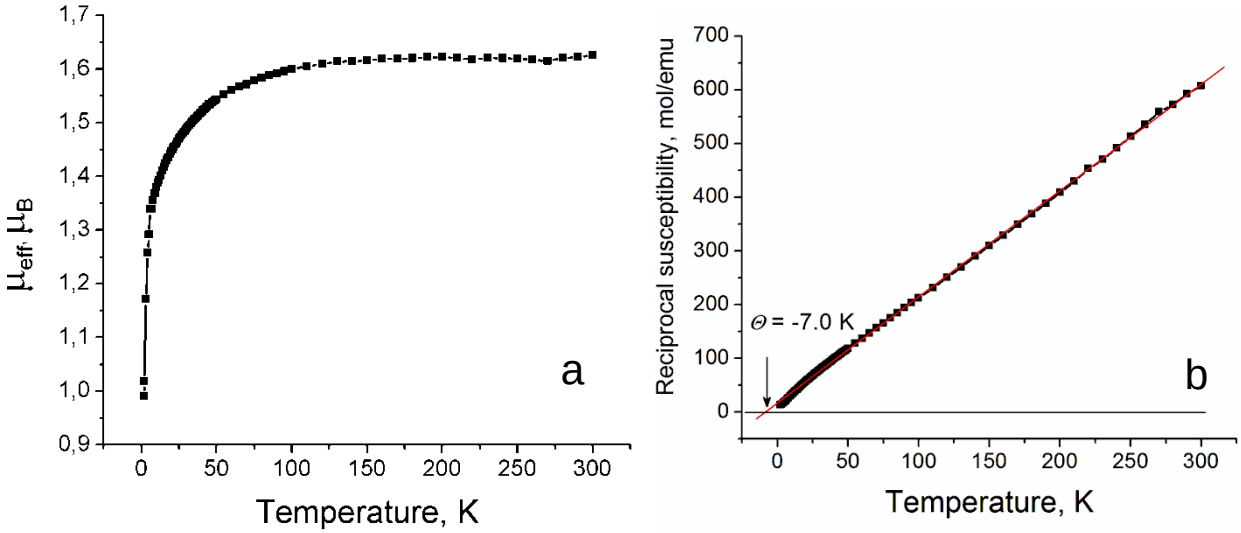

Figure S11. Temperature dependence of effective magnetic moment (a) and reciprocal molar magnetic susceptibility (b) for polycrystalline salt **3**.

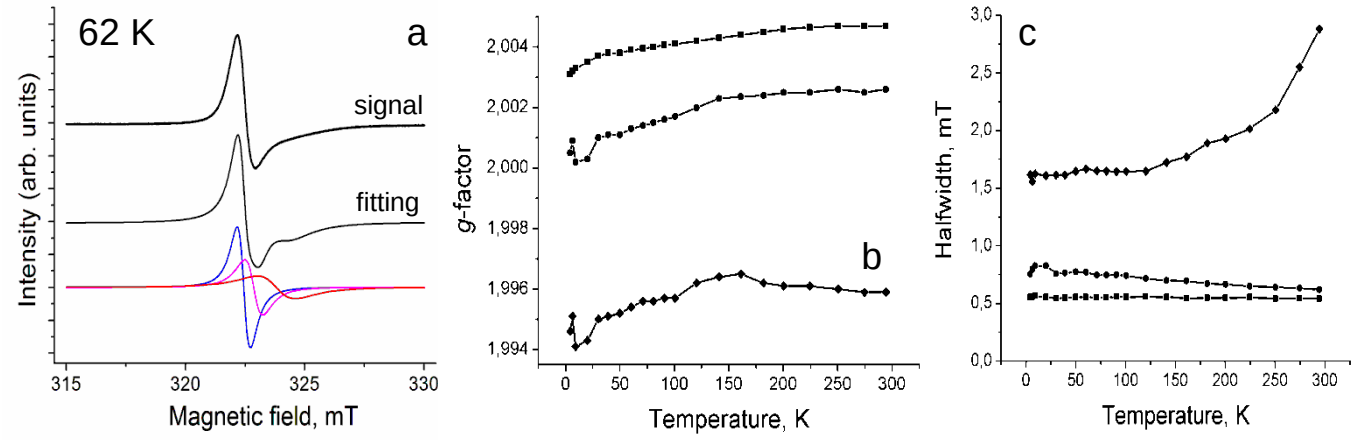

Figure S12. (a) EPR spectrum of polycrystalline **3** at 62 K. The fitting of the signal by three Lorentzian lines is shown below. Temperature dependencies of three components of EPR signal in **3**: *q*-factor (b) and linewidth (c).

.

{Cp*Mo(Br)(CO)$_2$[Sn^{II}Pc(2−)]}·0.5C$_6$H$_4$Cl$_2$ (1)

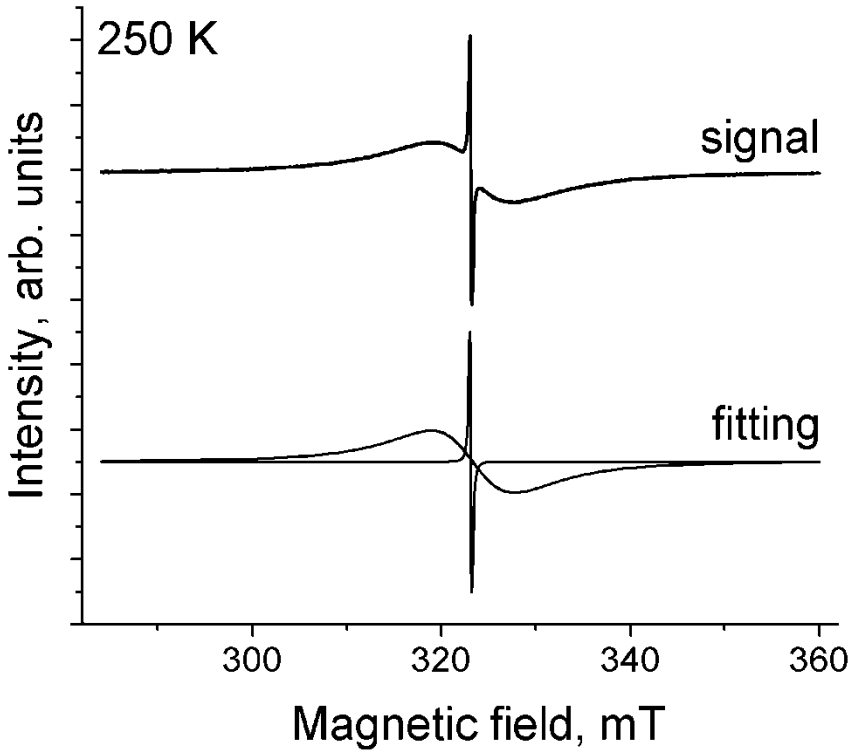

Figure S13. EPR signal from polycrystalline **1** at 250 K.

{Cryptand(Na$^+$)}{CpFe(CO)$_2$[Sn^{II}Pc(4–)]}$^-$·C$_6$H$_4$Cl$_2$ (4)

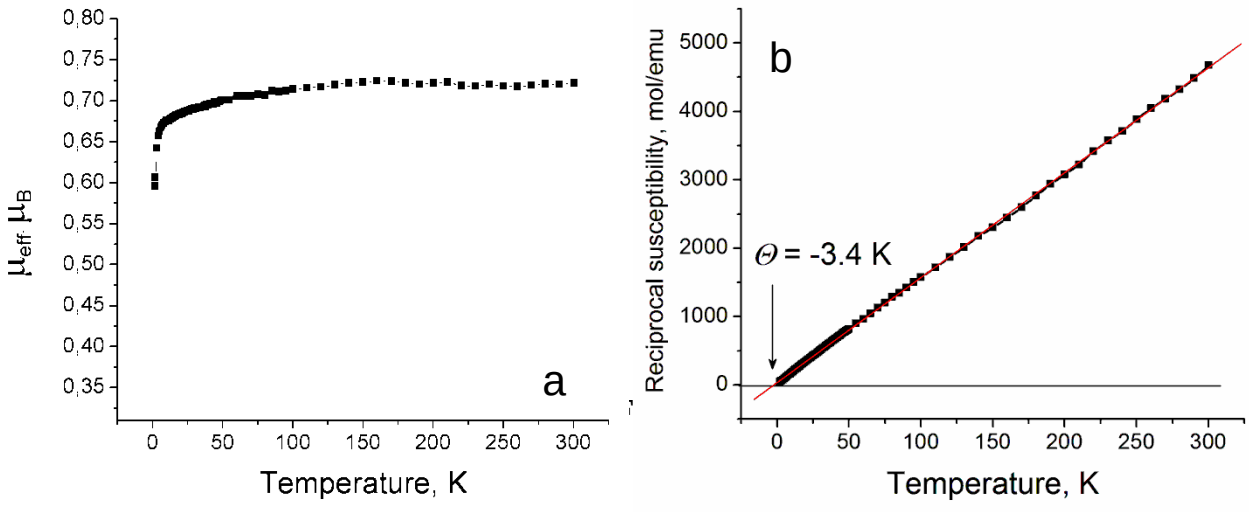

Figure S14. Temperature dependence of effective magnetic moment (a) and reciprocal molar magnetic susceptibility (b) for polycrystalline salt **4**.

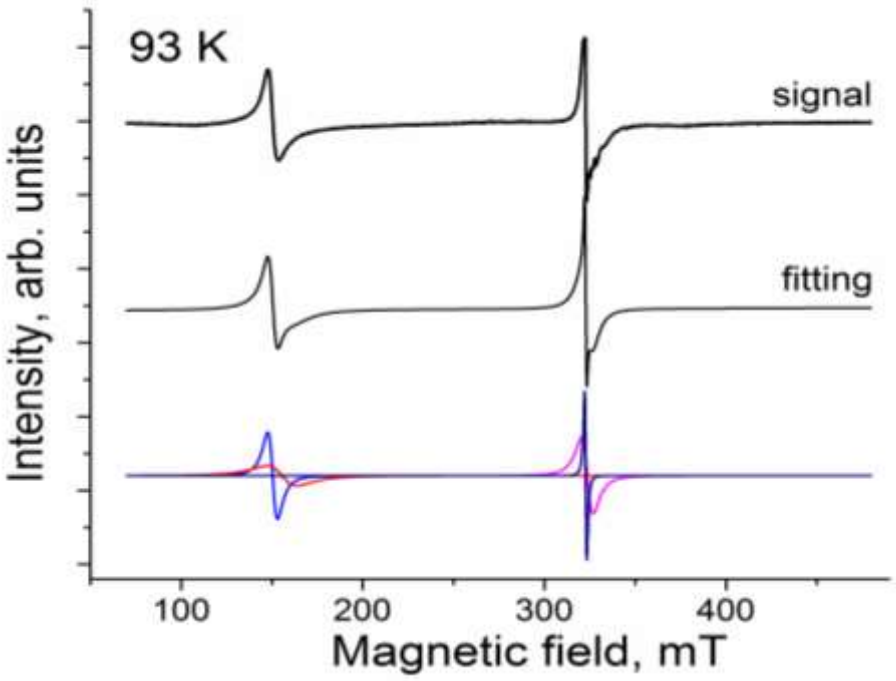

Figure S15. Weak EPR signal observed polycrystalline **4** at 93 K. The fitting of two components by two Lorentzian lines is shown below.

{Cryptand(Na^+)}{$Fe(CO)_4$[$Sn^{II}Pc(3-)]^{\bullet-}$}·1/3$C_6H_4Cl_2$ (5)

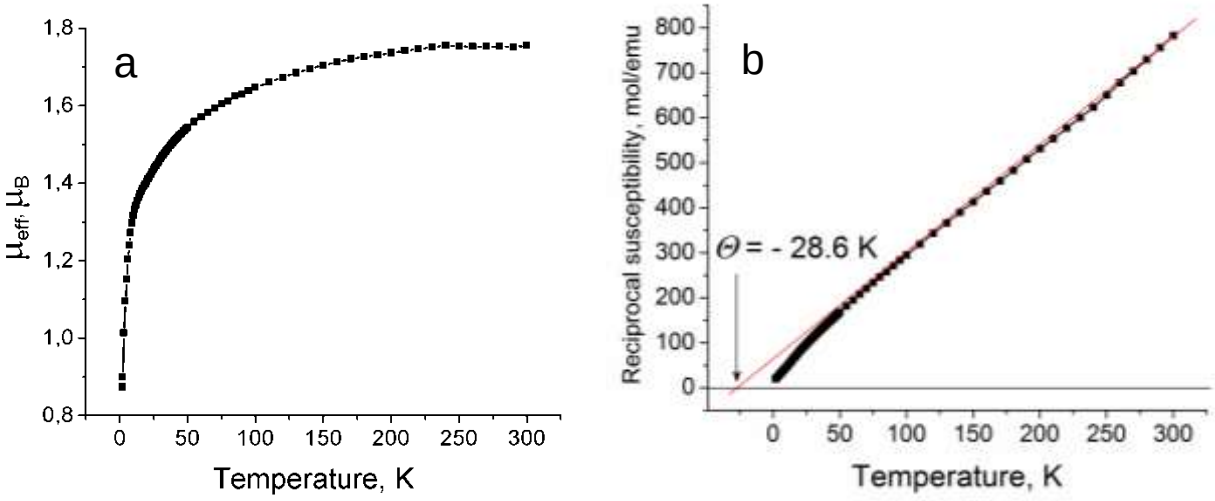

Figure S16. Temperature dependence of effective magnetic moment (a) and reciprocal molar magnetic susceptibility (b) for polycrystalline complex **5**.

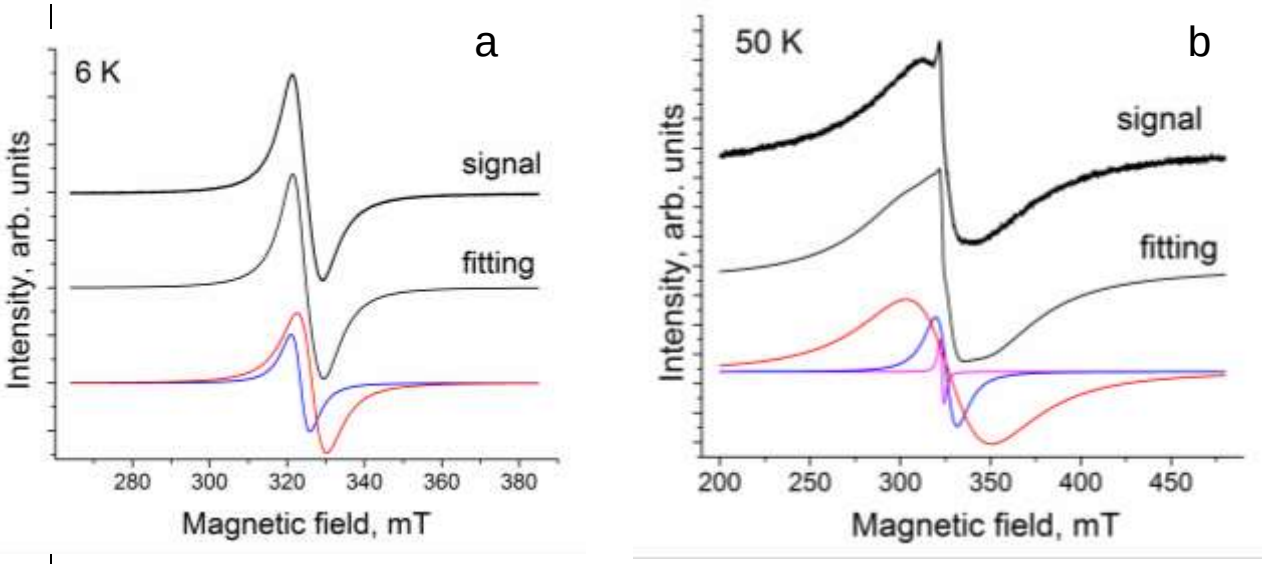

Figure S17. EPR signal from polycrystalline **5** at 6 (a) and 50 K (b). The fitting of the signals by two and three Lorentzian lines, respectively is shown below.

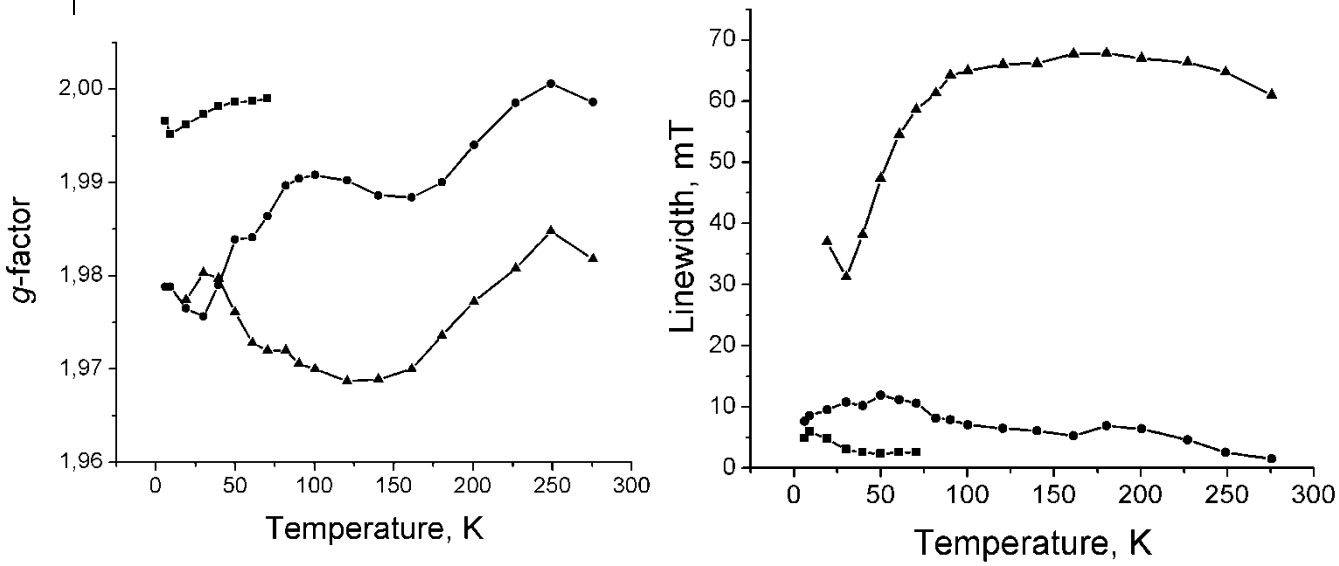

Figure S18. Temperature dependence of *g*-factors and linewidths of three components of EPR signal in **5**.

{Cryptand(Na^+)}{CpMo(CO)$_2$[Sn^{II}Pc(2–)Sn^{II}Pc(3–)$^{\bullet-}$]}·3.5$C_6H_4Cl_2$ (6)

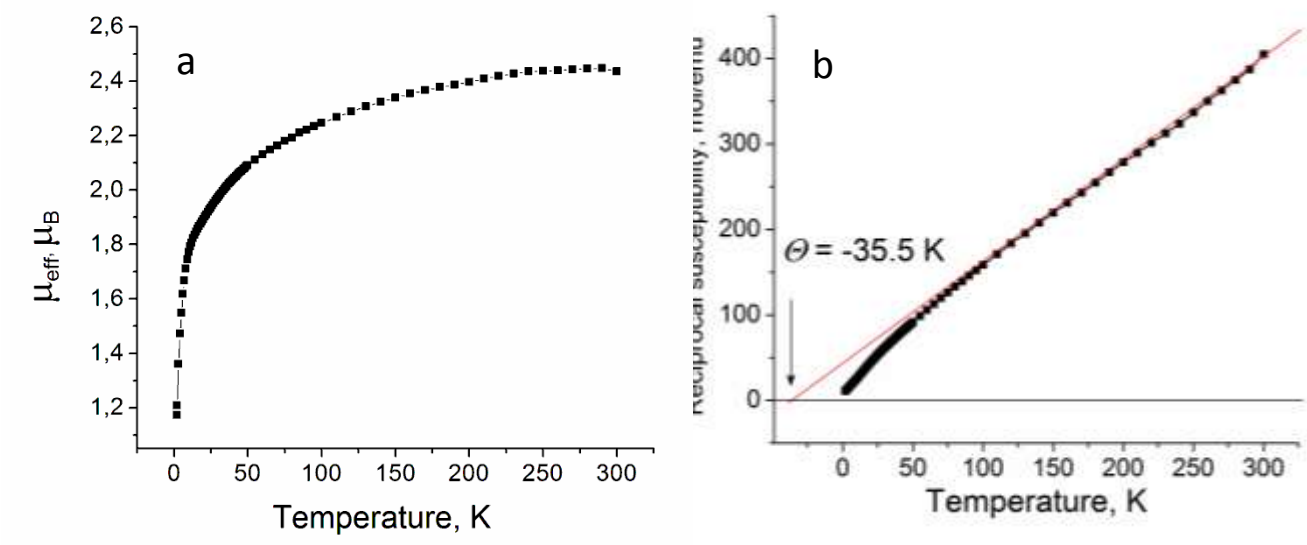

Figure S19. Temperature dependence of effective magnetic moment (a) and reciprocal molar magnetic susceptibility (b) for polycrystalline **6**.

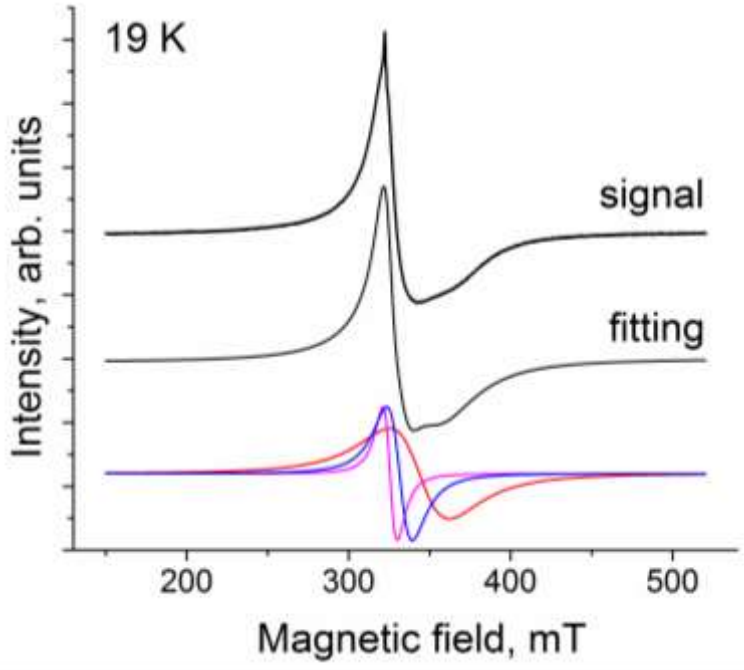

Figure S20. EPR signal from polycrystalline **6** at 19 K. The fitting of the signal by three Lorentzian lines is shown below.

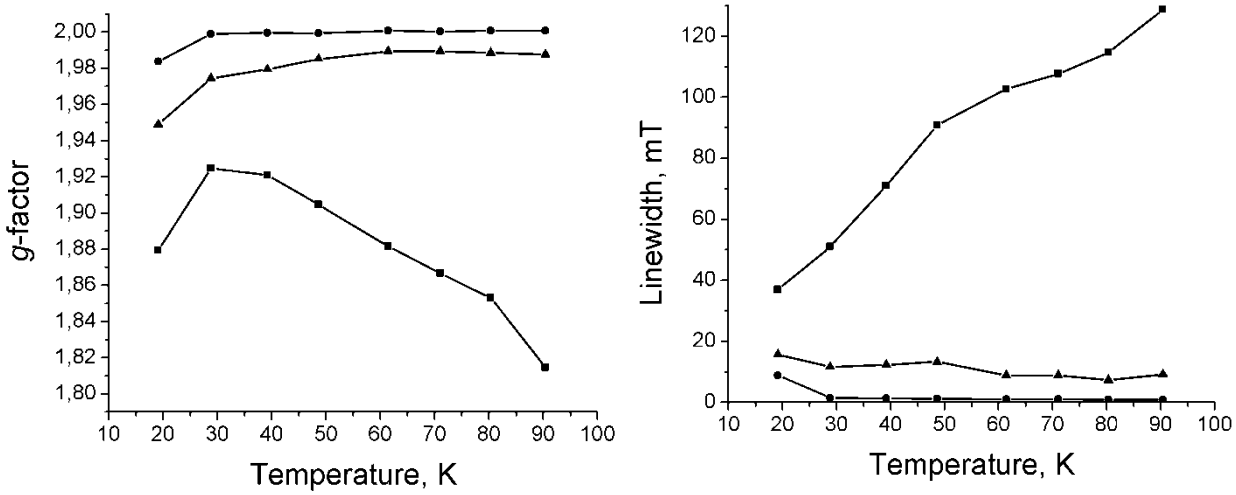

Figure S21. Temperature dependence of *g*-factors and linewidths of three components of EPR signal in **6**.

{Cryptand(Na^+)}{Cp*$RhCl_2$[Sn^{II}Pc(3−)]$^{\bullet-}$}·$C_6H_4Cl_2$ (7)

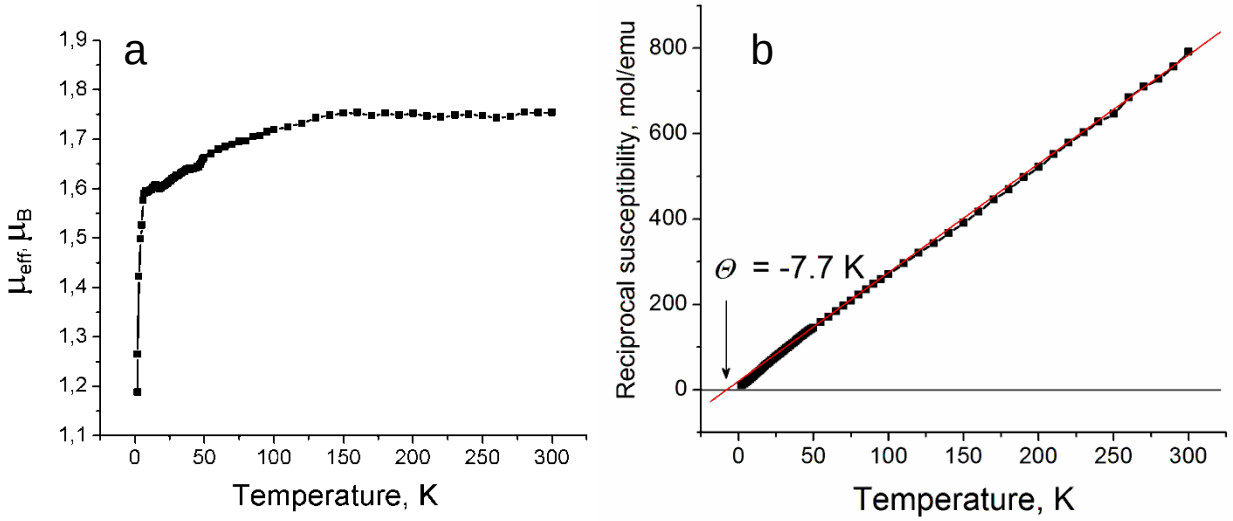

Figure S22. Temperature dependence of effective magnetic moment (a) and reciprocal molar magnetic susceptibility (b) for polycrystalline salt **7**.

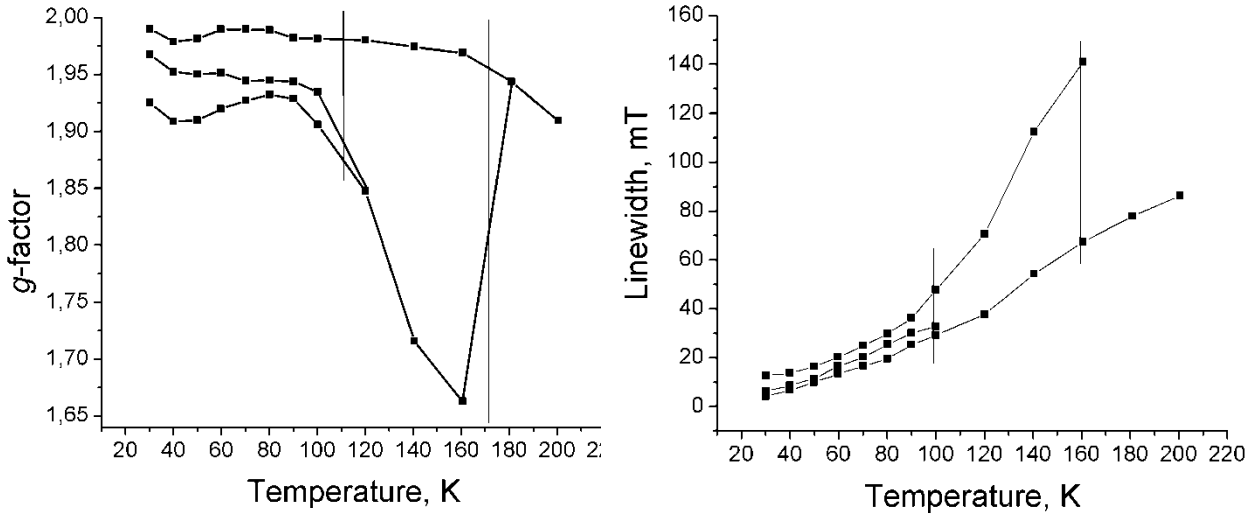

Figure S23. Temperature dependence of *g*-factors and linewidths of three components of EPR signal in **7**.

{$Ph_5CpRu(CO)_2[Sn^{II}Pc(3-)]$} (8).

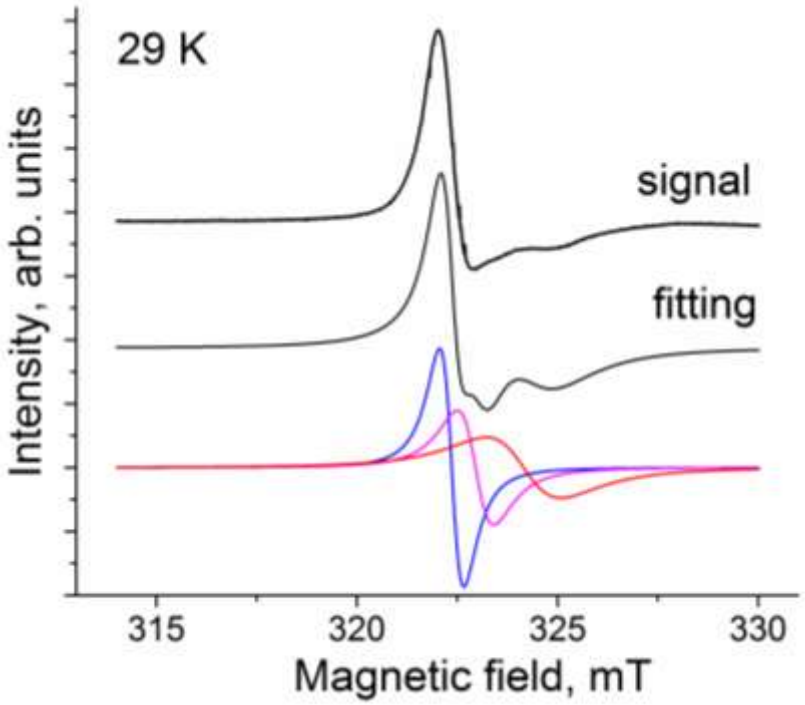

Figure S24. EPR signal from polycrystalline **8** at 29 K. The fitting of the signal by three Lorentzian lines is shown below.

Theoretical calculations.

Table S6.
Calculation method, point group (PG), state, total and relative energy (E and E_{rel}), and $<S^2>$ value of $[CpFe(CO)_2(SnPc)]^-$, $Ph_5CpRu(CO)_2(SnPc)$, and $[Ph_5CpRu(CO)_2(SnPc)]_2$ calculated at the M11/cc-pVTZ(-PP)/cc-pVDZ level of theory.

Method[a]	PG	State	E / hartree	E_{rel} / K	$<S^2>$
$[CpFe(CO)_2(SnPc)]^-$					
RM11//RM11[a]	C_1	^1A	−3564.28356	−3687	0
RM11//RM11[b]	C_1	^1A	−3564.27188	0	0
UM11//UM11[b]	C_1	^3A	−3564.23822	10630	2.019
UM11//UM11[b]	C_1	^5A	−3564.15503	36899	6.035
$Ph_5CpRu(CO)_2(SnPc)$					
UM11//UM11[b]	C_1	^2A	−3549.72165	0	0.824
UM11//UM11[b]	C_1	^4A	−3549.68701	10939	3.785
$[Ph_5CpRu(CO)_2(SnPc)]_2$					
UM11//UM11[b]	C_i	BS-singlet[c]	−7099.48911	0	1.194
UM11//UM11[b]	C_i	^3A_u	−7099.48816	299	2.219

[a] Full geometry optimization was done. [b] Only the coordinates of hydrogen atoms were optimized. [c] Broken-symmetry singlet.

Table S7.
Charge and spin densities of the ^1A state in $[CpFe(CO)_2(SnPc)]^-$, the ^2A state in $Ph_5CpRu(CO)_2(SnPc)$, and the broken-symmetry singlet state in $[Ph_5CpRu(CO)_2(SnPc)]_2$ by Mulliken and natural population analysis at the M11/cc-pVTZ(-PP)/cc-pVDZ level of theory.

	Charge		Spin	
	MPA[a]	NPA[b]	MPA[a]	NPA[b]
$[CpFe(CO)_2(SnPc)]^-$				
Fe	−0.305	−1.572		
Cp	0.231	0.325		
C(6)O(101)	0.049	0.469		
C(7)O(102)	0.025	0.462		
Sn	0.793	2.138		
Pc	−1.793	−2.822		
$Ph_5CpRu(CO)_2(SnPc)$				
Ru	−0.708	−1.244	0.003	0.000
Ph_5Cp	0.214	0.248	0.003	0.000
C(201)O(201)	0.260	0.439	−0.001	−0.001
C(202)O(202)	0.227	0.430	0.000	0.000
Sn	0.970	2.024	0.011	0.005
Pc	−0.963	−1.897	0.988	0.995
$[Ph_5CpRu(CO)_2(SnPc)]_2$				
Ru	−0.728	−1.220	0.003	0.000
Ph_5Cp	0.190	0.226	−0.001	0.001
C(201)O(201)	0.244	0.438	−0.001	−0.001
C(202)O(202)	0.212	0.428	0.000	0.000
Sn	1.067	2.080	0.010	0.004
Pc	−0.984	−1.952	0.968	0.971

[a] Mulliken population analysis. [b] Natural population analysis.

Table S8
Wiberg bond indices calculated at the M11/cc-pVTZ(-PP)/cc-pVDZ level of theory.

$[CpFe(CO)_2(SnPc)]^-$		$Ph_5CpRu(CO)_2(SnPc)$		$[Ph_5CpRu(CO)_2(SnPc)]_2$	
Fe−Sn	0.641	Ru−Sn	0.724	Ru−Sn	0.716
Total(Fe)	5.038	Total(Ru)	5.074	Total(Ru)	5.029
Total(Sn)	2.687	Total(Sn)	2.670	Total(Sn)	2.606

Table S9.

Selected bond lengths (Å) of the ^{1}A state in fully-geometry-optimized $[CpFe(CO)_2(SnPc)]^-$ at the RM11/cc-pVTZ(-PP)/cc-pVDZ level of theory.

	Calc.	Exp.
Fe–Sn	2.495	2.5087(5)
Fe–C(carbonyl)	1.778	1.758(3)
	1.785	1.767(3)
CO	1.143	1.148(4)
	1.141	1.143(4)
Fe–C(Cp)	2.120	2.095(3)
	2.114	2.094(3)
	2.103	2.097(3)
	2.097	2.104(3)
	2.107	2.098(3)

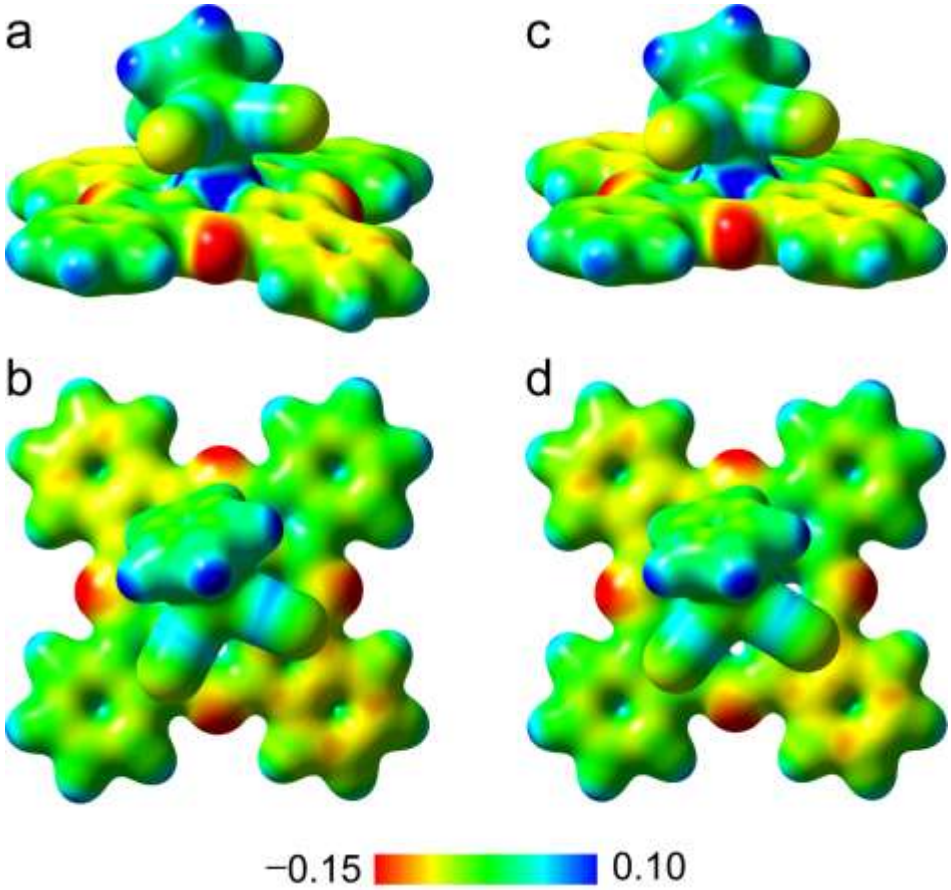

Figure S25. Electrostatic potential maps for (a,c) side and (b,d) top views on the 0.02 electron/au^3 of electron density surface for the ^1A state in (a,b) partially- and (c,d) fully-optimized $[CpFe(CO)_2(SnPc)]^-$ anion calculated at the RM11/cc-pVTZ(-PP)/cc-pVDZ level of theory.

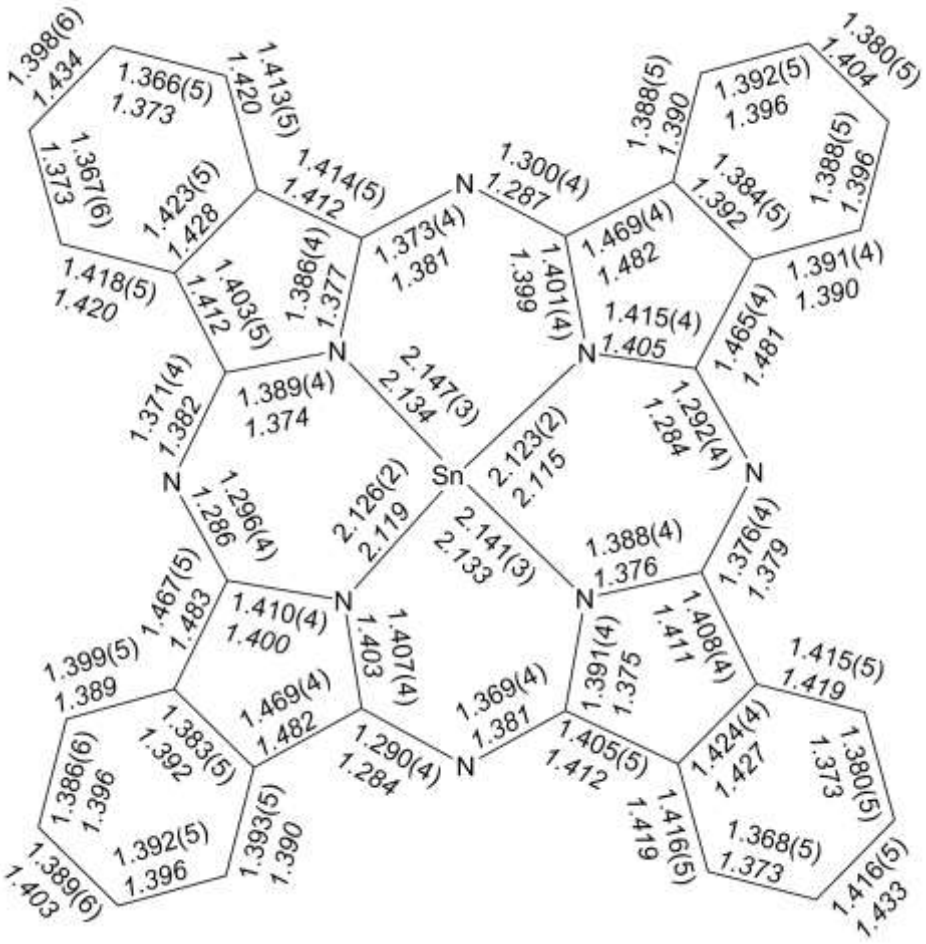

Figure S26. Experimental and calculated bond lengths (Å) of SnPc moiety in $[CpFe(CO)_2(SnPc)]^-$ anion. Calculated bond lengths are in italics. Full geometry optimization on $[CpFe(CO)_2(SnPc)]^-$ anion was carried out at the RM11/cc-pVTZ(-PP)/cc-pVDZ level of theory.

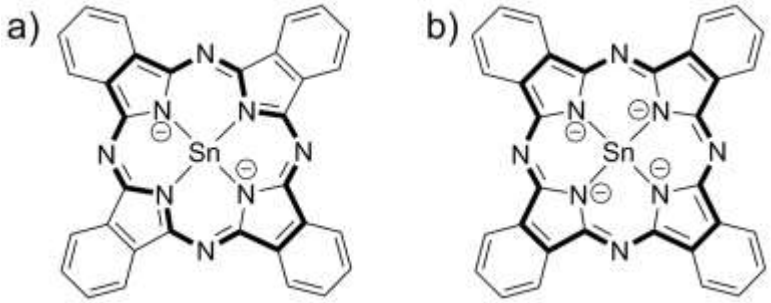

Figure S27. (a) $[SnPc]^0$ and (b) $[SnPc]^{2-}$ with 18 and 20 π-electronic phthalocyanine moieties, respectively.

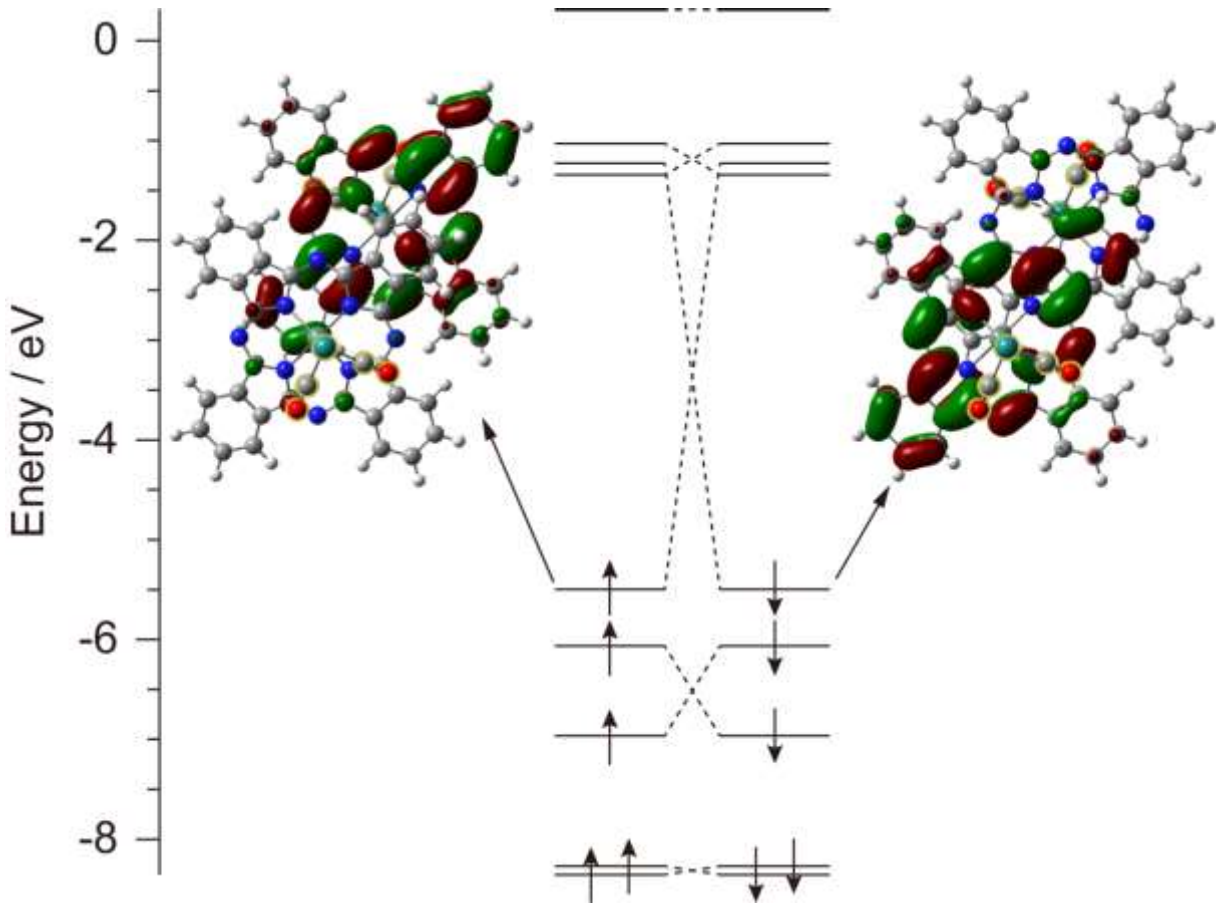

Figure S28. Energy diagram for the frontier Kohn-Sham orbitals of $[Ph_5CpRu(CO)_2(SnPc)]_2$ dimer in the broken-symmetry singlet state calculated at the UM11/cc-pVTZ-PP/cc-pVDZ level of theory. For clarity, the pentaphenylcyclopentadienyl ligand is omitted, and $Ru(CO)_2$ moieties are highlighted in α- and β-HO orbitals.

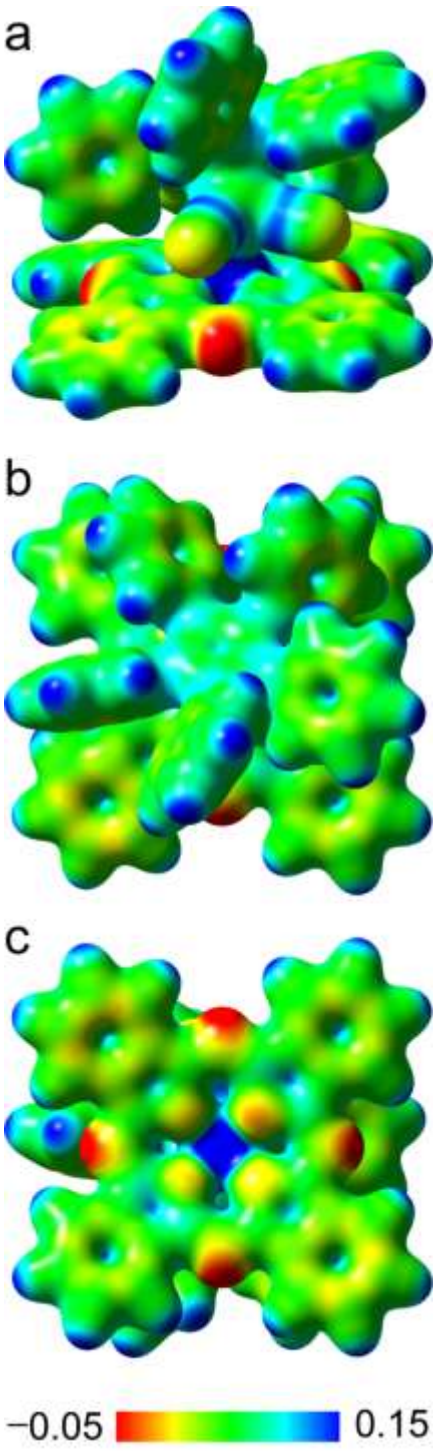

Figure S29. Electrostatic potential maps for (a) side, (b) top, and (c) bottom views on the 0.02 electron/au^3 of electron density surface for the ^2A state in $Ph_5CpRu(CO)_2(SnPc)$ monomer calculated at the UM11/cc-pVTZ(-PP)/cc-pVDZ level of theory.

Figure S30. Isosurface plot on spin density distribution of the ^2A state in $Ph_5CpRu(CO)_2(SnPc)$ monomer calculated at the UM11/cc-pVTZ-PP/cc-pVDZ level of theory. The isosurface value is 0.0009 electron/au^3, and the isosurfaces in blue and green denote the positive and negative spin density, respectively. For clarity, pentaphenylcyclopentadienyl ligand is omitted.

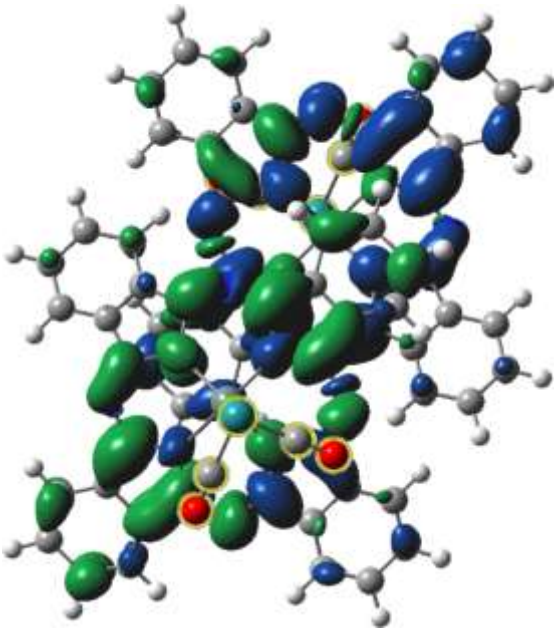

Figure S31. Isosurface plot on spin density distribution of the broken-symmetry singlet state in $[Ph_5CpRu(CO)_2(SnPc)]_2$ dimer calculated at the UM11/cc-pVTZ-PP/cc-pVDZ level of theory. The isosurface value is 0.0009 electron/au^3, and the isosurfaces in blue and green denote the positive and negative spin density, respectively. For clarity, pentaphenylcyclopentadienyl ligand is omitted, and $Ru(CO)_2$ moieties are highlighted.